Assessing the Convective Environment over Irrigated and Nonirrigated Land Use with Land–Atmosphere Coupling Metrics: Results from GRAINEX

DANIEL WHITESEL,[a,b,c] REZAUL MAHMOOD,[a,c] CHRISTOPHER PHILLIPS,[d] JOSHUA ROUNDY,[e] ERIC RAPPIN,[f] PAUL FLANAGAN,[g] JOSEPH A. SANTANELLO JR.,[h] UDAYSANKAR NAIR,[d] AND ROGER PIELKE SR.[i,j]

[a] *High Plains Regional Climate Center, University of Nebraska–Lincoln, Lincoln, Nebraska*
[b] *National Drought Mitigation Center, University of Nebraska–Lincoln, Lincoln, Nebraska*
[c] *School of Natural Resources, University of Nebraska–Lincoln, Lincoln, Nebraska*
[d] *Department of Atmospheric Science, University of Alabama in Huntsville, Huntsville, Alabama*
[e] *Department of Civil, Environmental, and Architectural Engineering, University of Kansas, Lawrence, Kansas*
[f] *Kentucky Climate Center, Western Kentucky University, Bowling Green, Kentucky*
[g] *U.S. Department of Agriculture, Agricultural Research Service, El Reno, Oklahoma*
[h] *Hydrological Sciences Laboratory, NASA Goddard Space Flight Center, Greenbelt, Maryland*
[i] *Department of Atmospheric and Oceanic Sciences, University of Colorado Boulder, Boulder, Colorado*
[j] *CIRES, University of Colorado Boulder, Boulder, Colorado*

(Manuscript received 31 October 2023, in final form 24 February 2024, accepted 29 April 2024)

ABSTRACT: Land-use land-cover change affects weather and climate. This paper quantifies land–atmosphere interactions over irrigated and nonirrigated land uses during the Great Plains Irrigation Experiment (GRAINEX). Three coupling metrics were used to quantify land–atmosphere interactions as they relate to convection. They include the convective triggering potential (CTP), the low-level humidity index (HI_{low}), and the lifting condensation level (LCL) deficit. These metrics were calculated from the rawinsonde data obtained from the Integrated Sounding Systems (ISSs) for Rogers Farm and York Airport along with soundings launched from the three Doppler on Wheels (DOW) sites. Each metric was categorized by intensive observation period (IOP), cloud cover, and time of day. Results show that with higher CTP, lower HI_{low}, and lower LCL deficit, conditions were more favorable for convective development over irrigated land use. When metrics were grouped and analyzed by IOP, compared to nonirrigated land use, HI_{low} was found to be lower for irrigated land use, suggesting favorable conditions for convective development. Furthermore, when metrics were grouped and analyzed by clear and nonclear days, CTP values were higher over irrigated cropland than nonirrigated land use. In addition, compared to nonirrigated land use, the LCL deficit during the peak growing season was lower over irrigated land use, suggesting a favorable condition for convection. It is found that with the transition from the early summer to the mid/peak summer and increased irrigation, the environment became more favorable for convective development over irrigated land use. Finally, it was found that regardless of background atmospheric conditions, irrigated land use provided a favorable environment for convective development.

KEYWORDS: Atmosphere–land interaction; Climate; Hydrometeorology; Mesoscale processes; Soil moisture; Diurnal effects

1. Introduction and background

Land-use land-cover change (LULCC) is an important driver of regional weather and climate (Pielke et al. 2011; Mahmood et al. 2010, 2014; Cook et al. 2020; McDermid et al. 2023). Human activities, such as deforestation, urbanization, and agriculture, are the main drivers of LULCC. LULCC impacts the surface energy balance, moisture budgets, and other land surface properties (Pielke et al. 2016), which can lead to changes in local and regional atmospheric circulations, temperature, and precipitation (Mahmood et al. 2004, 2006, 2011, 2013; Shukla et al. 2014; Fan et al. 2015a,b; Xu et al. 2015; Mueller et al. 2016, 2017; Winchester et al. 2017; Singh et al. 2018; Rodgers et al. 2018; Chen and Dirmeyer 2019; Nair et al. 2019; Zhang et al. 2019; Hu et al. 2019; Flanagan et al. 2021; McDermid et al. 2021; Rappin et al. 2021, 2022; Phillips et al. 2022).

Irrigated agriculture is in high demand, due to the increasing need for food (McDermid et al. 2023). Two effects are found to be common with irrigation's application: an increase in evapotranspiration (ET) and a decrease in air temperatures (Mahmood and Hubbard 2002; Mahmood et al. 2004, 2006; DeAngelis et al. 2010; Cook et al. 2011, 2015, 2020; Sen Roy et al. 2007, 2011; Alter et al. 2015, 2018; Pei et al. 2016; McDermid 2019; Yang et al. 2019; Rappin et al. 2021). With an increase in ET come increases in latent heat flux and decreases in sensible heat flux, thereby changing the surface energy balance (Mahmood et al. 2013; Rappin et al. 2021). The decrease in sensible heat flux results in lower maximum air temperatures. Analysis of long-term observed temperature database studies suggests that over the Great Plains, compared to nonirrigated areas and during the growing season, irrigation resulted in 1.01°C cooling of mean maximum temperature

Supplemental information related to this paper is available at the Journals Online website: https://doi.org/10.1175/JHM-D-23-0187.s1.

Corresponding author: Rezaul Mahmood, rmahmood2@unl.edu

DOI: 10.1175/JHM-D-23-0187.1

(Mahmood et al. 2004, 2006, 2013) In addition, Bonfils and Lobell (2007) found ~0.20°C decade^{-1} cooling trends in temperature over irrigated areas during the growing season in Nebraska. Analysis of growing season observed data found up to 2.17°C increased dewpoint temperatures over irrigated areas (Mahmood et al. 2008). In an observational database study for California, Christy et al. (2006) found a 0.26°C decade^{-1} cooling of growing season maximum temperature due to irrigation. In a subsequent study, Lawston et al. (2020) found up to 1.68°C cooling of mean maximum summer temperature in the Pacific northwestern United States due to irrigation. Furthermore, historical observed data analysis suggests up to 0.34°C cooling of growing season maximum temperatures over irrigated areas in India (Sen Roy et al. 2007). The same study found up to 0.53°C cooling of temperature during individual growing season months. In a recent research, Kang and Eltahir (2019) found that the surface temperature decreased by 0.43°C due to irrigation in the north central plains of China.

However, irrigation's effects on precipitation are more complex. An observational data based study suggests that precipitation can be reduced in the immediate area due to the decrease in sensible heat lowering the likelihood of cloud formation by reducing turbulent transfer (Szilagyi and Franz 2020). Furthermore, observed historical data suggest that in regions downwind, irrigation can potentially increase precipitation (Barnston and Schickedanz 1984). Sen Roy et al. (2011) found up to 69-mm (121%) increase in total precipitation for growing seasons due to irrigation in northwestern India. It is also found that over the North China Plain precipitation increased by 1.25 mm day^{-1} after the full implementation of irrigation (Kang and Eltahir 2019).

Irrigation increases soil moisture, and a significant amount of research has been conducted in the past focusing on soil moisture and its role in land–atmosphere (L–A) interactions (e.g., Ookouchi et al. 1984; Eltahir 1998; Findell and Eltahir 2003a,b; Leeper et al. 2011; Mahmood et al. 2012; Suarez et al. 2014; Santanello et al. 2018). These studies assessed, among others, the evolution of the planetary boundary layer (PBL) and related boundary layer processes, the role of surface fluxes in the PBL development, and changes in various convective parameters such as the lifting condensation level (LCL) and the level of free convection (LFC). Soil moisture impacts the surface energy and water budgets through changes to the albedo and Bowen ratio (the ratio of the surface sensible heat flux to the latent heat flux, or ET) or evaporative fraction [EF, the ratio of the latent heat flux to the net surface flux (i.e., net radiative flux)]. The wetter the soil, the greater the amount of incoming radiation energy is partitioned into ET, leading to relatively smaller values of atmospheric sensible heat flux and a larger EF. Depending on the specific humidity of the PBL, ET from moist soil can be static or change in magnitude over multiple time scales. For example, as ET occurs and the PBL moistens, the magnitude of EF reduces. Large-scale circulations can therefore have a significant impact on a process chain for L–A interactions proposed by Santanello et al. (2018) where moist (dry) advection over wet soil can reduce (increase) the magnitude of ET. On the other hand, it is the soil moisture that controls the partitioning between sensible and latent heat fluxes. When soils are wet, the latent heat flux is determined by the available net radiation and latent heat fluxes dominate, whereas when the soil is dry, the availability of moisture controls the degree of latent heating, which is depressed at the expense of sensible heat fluxes.

Just as soil moisture (from irrigation or precipitation) exerts a strong control on the EF, the EF exerts a strong control on the PBL's growth and decay. Low values of EF (e.g., large sensible heat flux) support PBL growth, while a large EF will significantly reduce PBL growth due to a weak buoyant heat flux. In summary, sensible heating and small EF help to grow the PBL, while latent heating moistens the PBL but may not necessarily grow it to the LCL. The role of surface fluxes and their influence on the PBL structure and evolution were further discussed by Santanello et al. (2007, 2009, 2011, 2013, 2018, 2019). This understanding is further supported by McPherson (2007), as she noted that the strength of land–atmosphere interactions is sensitive to potential ET and surface physical conditions including soil moisture. Holt et al. (2006) suggested that the modification of soil moisture (e.g., by irrigation) changes emissivity and albedo which subsequently affect L–A interactions via changes in sensible and latent energy partitioning, air temperature, and PBL moisture content. The response propagates upward through the boundary layer via turbulent transport and affects boundary layer growth, convective initiation, and precipitation amounts.

It is noted that wet soils can lead to a shallow boundary layer and a large moist entropy per unit mass (Eltahir 1998). As a result, a low LFC combined with high boundary layer specific humidity may result in positive soil moisture/evaporation–cloud formation feedback. Conversely, over regions of dry soil the sensible heat flux dominates the latent heat flux (large Bowen ratio) and can hinder cloud development. Overall, given the existence of both positive and negative soil moisture–cloud development feedbacks, it is not surprising that both positive and negative soil moisture–precipitation (hence, irrigation–precipitation) feedbacks have also been identified (e.g., Ford et al. 2015a,b). The positive feedback, in which precipitation forms preferentially over wet soils, has been found in one-dimensional idealized models (Eltahir 1998; Findell and Eltahir 2003a,b,c) as well as in three-dimensional mesoscale models (Schlemmer et al. 2011, 2012) and observations (Betts and Ball 1998; Taylor 2010; Berg et al. 2013).

The entire process link chain proposed by Santanello et al. (2018) is bookmarked by the relationship between soil moisture and precipitation, termed the soil moisture–precipitation (SM–P) feedback (or termed as irrigation–precipitation for our purpose). There are numerous complexities to local soil moisture–ET–convective initiation–precipitation feedback. Furthermore, a relatively large Bowen ratio leads to a deep boundary layer and elevated LCL. In the absence of sufficient moisture, the LFC will not descend to the lifting condensation level and shallow convection as opposed to deep convection will develop. On the other hand, irrigation-induced increases in soil moisture would result in stronger latent energy fluxes and a smaller Bowen ratio. These factors would result in a shallow boundary layer with large moist static energy such

that subsequent large-scale forcing would lead to significant additional precipitation.

Research suggests that thunderstorm severity may be enhanced due to differential heating between areas of moist and adjacent dry, vegetated land (Segal et al. 1988; Pielke and Zeng 1989). Moreover, soil moisture enhancement due to agriculture and irrigation significantly impacts weather and climate (e.g., Puma and Cook 2010; Wei et al. 2013). Excellent examples of the impacts of increased soil moisture due to irrigation can be found in the Great Plains (GP) of North America (Barnston and Schickedanz 1984; Mahmood and Hubbard 2002; Adegoke et al. 2003; DeAngelis et al. 2010; Harding and Snyder 2012a,b; Lawston et al. 2015).

Irrigation-induced increases in soil moisture can also be a good indicator of the location of deep convection (Findell and Eltahir 2003a,b; Frye and Mote 2010). Findell and Eltahir (2003a,b) utilized the convective triggering potential (CTP) and low-level humidity index (HI_{low}) to determine where deep convection would initiate with respect to soil moisture, using morning balloon sounding data. Additionally, studies suggest that there is a negative relationship between soil moisture and LCL deficits (Santanello et al. 2011). In other words, wetter soils lead to lower LCL deficits than drier soils. This can provide favorable conditions for cloud formation over wetter soils, even with the reduction in turbulent transfer over wetter soils.

In this context, the Great Plains Irrigation Experiment (GRAINEX) aimed to better understand L–A interactions between irrigated and nonirrigated croplands (Rappin et al. 2021). It was found that irrigated land use lowers near-surface maximum air temperature, increases dewpoint temperature, lowers PBL heights (PBLHs), and produces higher latent and lower sensible heat fluxes than nonirrigated cropland (Rappin et al. 2021, 2022; Lawston-Parker et al. 2023; Lachenmeier et al. 2024). Further analysis of GRAINEX data found that the irrigated land use weakens baroclinicity and mesoscale upslope circulations in the GP and potentially influences the GP low-level jet (Phillips et al. 2022).

The overall goal of this paper is to further understand the changes in the convective environment over irrigated and nonirrigated land uses by utilizing three coupling metrics. These metrics include CTP, HI_{low}, and LCL deficit (Findell and Eltahir 2003a,b; Ferguson and Wood 2011; Santanello et al. 2018). These metrics allowed us to identify environments favorable for convection. A key advantage of the current study is the use of a large number of radiosonde observations launched throughout the day including the typical periods of convective development. These launches were conducted during two distinct periods of crop/vegetation growth and irrigation application. Findell and Eltahir (2003a,b) used morning-only soundings in conjunction with a modeling framework, while Ferguson and Wood (2011) primarily used satellite data to explore L–A interactions. As such, this work provides a new perspective on L–A interactions over irrigated and nonirrigated land uses and soil moisture gradients (wet–dry) utilizing in situ observations. In addition, this research is complementary to Lachenmeier et al. (2024) where the authors investigated the impacts of irrigation on the PBLH, LCL, LFC, and PBL mixing ratio. It is found that irrigation lowers PBLH, LCL, and LFC and increases PBL mixing ratio.

In the context of these interactions between the land and atmosphere and the objectives of this research, the following sections of the paper provide further background on L–A interactions and discuss data used from the GRAINEX, methods applied to data, results, analysis and assessment of the findings, and conclusions.

2. Data and methods

a. *The GRAINEX field campaign and observations*

A detailed description of the GRAINEX field campaign, the data collected, and the observation platforms used is provided in Rappin et al. (2021). Hence, only a brief description is provided here. Data collection was completed from late May through early August 2018 over southeast Nebraska. Specifically, the field campaign was completed across two 15-day periods during the growing season of 2018: from 30 May through 13 June, known as the intensive observation period 1 (IOP1); and from 16 July through 30 July, known as the IOP2. Nebraska, located in the northern part of the North American GP, is one of the most extensively irrigated regions in the world (Bonfils and Lobell 2007; Lobell and Bonfils 2008). In southeast Nebraska (Fig. 1), nonirrigated land use (eastern part of the study area) transitions to irrigated land use (western part of the study area) as water from the High Plains aquifer becomes available for extraction. This transition also follows the east-to-west declining precipitation gradient of the North American GP. Common crops in the study area are corn and soybeans. During the field campaign, both IOP1 (late spring/beginning of the summer) and IOP2 (midsummer) experienced several rain events and periods of cooler and drier days (Rappin et al. 2021).

Data collection was completed by using a variety of observational platforms including 12 eddy covariance Integrated Surface Flux Systems (ISFSs) (NCAR Earth Observing Laboratory 1990), two Integrated Sounding Systems (ISSs) (NCAR Earth Observing Laboratory 1997), three Doppler on Wheels (DOW) mobile radar units (Wurman et al. 2021), and 75 Environmental Monitoring, Economical Sensor Hubs (EMESHs) (Rappin et al. 2021). In addition, a Twin Otter aircraft mounted with radiometers was flown over the study area by the National Aeronautics and Space Administration (NASA), which collected soil moisture data. Our current paper focuses on data from the ISS and DOW. Thus, a discussion on data from ISFS, EMESH, and NASA is not provided.

b. *ISSs*

As noted previously, there were two ISS sites from where rawinsonde balloons were launched throughout IOP1 and IOP2. Land use around one ISS site (ISS3 at York) was irrigated agriculture, while the other one (ISS2 at Rogers Farm) was nonirrigated agriculture. For each location, the first balloon was launched around 0500 local standard time (LST)

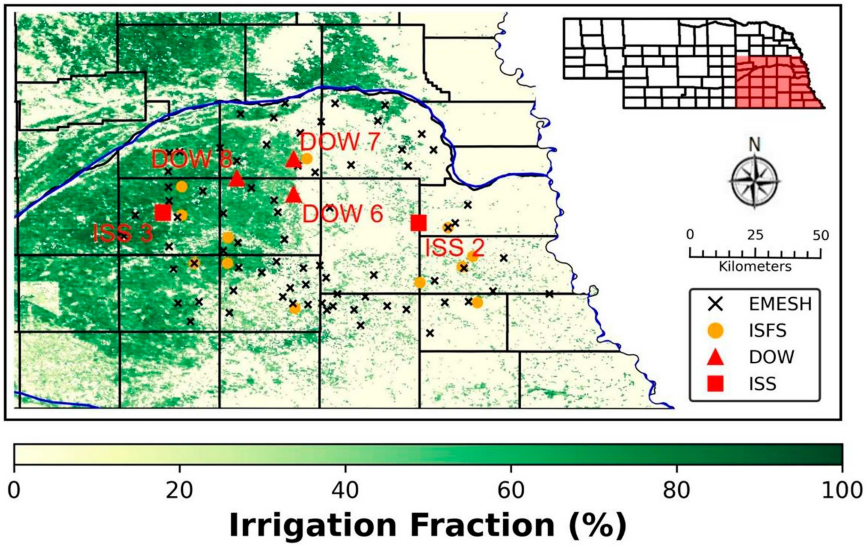

FIG. 1. Map of the GRAINEX study area in southeast Nebraska. Data collection sites consisted of 12 ISFSs, 2 ISSs, 3 DOW deployment locations, and 75 EMESHs.

[0600 local time (LT); 1100 UTC] and the last launch was around 1900 LST (2000 LT; 0100 UTC, next day). They were launched simultaneously every 2 h and every day during IOP1 and IOP2. Hence, 16 balloons were launched every day, and overall, 480 launches (8 launches × 2 sites × 30 days) were completed from the two sites. In short, this field campaign provided the most comprehensive dataset of this type for investigation into the impacts of land use, including irrigation, on the atmosphere.

c. *DOW*

Rawinsondes from three DOW locations were also launched simultaneously with the ISS launches (8 launches × 3 sites × 30 days = 720 launches). In total, about 1200 rawinsonde launches (ISS + DOW sites) were completed. DOW8 was located over irrigated land use, DOW7 was over nonirrigated, and DOW6 was in a transitional area. For additional details regarding all observation platforms and instrumentation, please consult Rappin et al. (2021) and see https://www.eol.ucar.edu/field_projects/grainex.

d. *Calculation of convective triggering potential, low-level humidity index, and LCL deficit*

Calculations of CTP, HI_{low}, and LCL deficit were completed for ~1050 soundings from the two ISS locations and the three DOW locations (EOL 2020). This study was focused on the morning [0700–1100 LST (1300–1700 UTC)] and afternoon [1300–1900 LST (1900–0100 UTC)] when L–A interactions can be effectively captured by the rawinsonde dataset. The formulation from Ferguson and Wood (2011) was used to calculate CTP and HI_{low}. These metrics were originally designed for morning soundings to capture the boundary layer properties prior to the onset of daytime land surface fluxes and to address the limitations of sounding launch frequency from the National Weather Service (one in the morning and one in the late afternoon). However, the wealth of sounding data from GRAINEX allowed for the calculation of CTP and HI_{low} every 2 h, which provides a unique perspective on how CTP and HI_{low} evolve during the day. Ferguson and Wood (2011) defined CTP (J kg^{-1}) as the integral of the area between the temperature sounding profile T_{env} (K) and a moist adiabat T_{parcel} (K) raised from the observed temperature and humidity 100 hPa (~1 km) above ground level (AGL) to a level 300 hPa (~3 km) AGL. AGL CTP can be expressed as follows:

$$\mathrm{CTP} = g\int_{Z_{\mathrm{PSurfStd}-300}}^{Z_{\mathrm{PSurfStd}-100}} \left(\frac{T_{\mathrm{parcel}} - T_{\mathrm{env}}}{T_{\mathrm{env}}}\right) dz. \tag{1}$$

In this Eq. (1), g is the gravitational acceleration (9.807 m s^{-2}) and dz is the thickness (m) of the layer.

Based on Eq. (1), it can be stated that the CTP assists in understanding lower-tropospheric stability by measuring the departure of the temperature profile from moist adiabatic conditions in the region between 100 and 300 hPa (~1–3 km) AGL (Findell and Eltahir 2003a,b; Santanello et al. 2018). When the actively growing daytime PBL reaches the LFC, deep convection can develop with sufficient moisture. For convective triggering, it is noted that PBL moistening and a simultaneous rapid lowering of the LFC are a more effective mechanism for convective development when the lower atmosphere is near moist adiabatic, and CTP is low (Santanello et al. 2018). On the other hand, high sensible heat flux and rapid PBL growth are more effective for convection development when the low-level atmospheric profile is near dry adiabatic, and the CTP is high. Overall, a negative CTP suggests that the local atmosphere is too stable for convection to develop (Findell and Eltahir 2003a).

Subsequently, following the formulation of Ferguson and Wood (2011), HI_{low} is calculated as the sum of the dewpoint

TABLE 1. CTP–HI_{low} framework categories (following Findell and Eltahir 2003a).

Category	Conditions	Box color
Atmospherically controlled; too dry for rain	CTP > 0, $HI_{low} \geq 15$	Red
Atmospherically controlled; too stable for rain	CTP < 0	Green
Atmospherically controlled; precipitation occurs in both wet and dry soils	CTP > 0, $0 < HI_{low} < 5$	Dark blue
Transition zone	$50 < CTP < 200$, $10 < HI_{low} < 15$	Gray
Wet soil advantage	CTP > 0, $5 < HI_{low} < 10$	Blue
Dry soil advantage	CTP > 200, $10 < HI_{low} < 15$	Yellow

depressions at 50- and 150-hPa pressure AGL and can be expressed as follows:

$$HI_{low} = (T_{PSurfStd\text{-}50} - T_{d,PSurfStd\text{-}50}) + (T_{PSurfStd\text{-}150} - T_{d,PSurfStd\text{-}150}). \quad (2)$$

In Eq. (2), $T_{PSurfStd\text{-}p}$ and $T_{d,PSurfStd\text{-}p}$ are the temperature and dewpoint temperature at pressure p AGL, respectively.

When HI_{low} indicates that lower atmosphere is extremely dry (higher value of HI_{low}), then moisture from the surface evaporated into the PBL will not be available for sufficiently enhancing the moist static energy of the PBL for convection to occur (Findell and Eltahir 2003a,b; Santanello et al. 2018). These types of days are identified as atmospherically controlled when rain cannot be initiated by local surface processes. Likewise, if the HI_{low} is close to zero, it is also atmospherically controlled due to a very moist atmosphere, which will likely lead to convection regardless of land surface controls. Note that lower HI_{low} values suggest a moister environment. Various ranges of favorable HI_{low} for different underlying conditions are provided in Table 1 in the following section.

The LCL deficit is the difference between the LCL and the PBLH. This metric was designed to measure the deficiencies in the growth of the planetary boundary layer due to a lack of mixing of heat and moisture (Santanello et al. 2011). Larger LCL deficit values indicate such deficiencies in the PBL growth. However, when the LCL deficit is zero or negative, the PBL has developed past the LCL and clouds will readily form within the PBL. During wet coupling, PBLH and LCL both can be lowered, resulting in smaller LCL deficits due to higher latent heat flux and lower sensible heat flux over irrigated areas and providing conditions for convection, cloud development, and precipitation. Under dry coupling, the LCL deficit can be lower due to higher PBLH linked to an increase in sensible heat flux (Roundy and Santanello 2017). LCL deficits were calculated every 2 h along with CTP and HI_{low}.

e. *CTP–HI_{low} framework and LCL deficit*

CTP values and corresponding HI_{low} values were categorized following the framework of Findell and Eltahir (2003a) and presented in Table 1. To further illustrate their role in L–A interactions, they are also presented graphically in Fig. 2.

These categories presented in Table 1 can further be presented as follows.

Subsequently, CTP and HI_{low} were analyzed along with LCL deficit for irrigated and nonirrigated land uses for IOPs (i.e., IOP1 and IOP2), cloud cover (clear and nonclear days), clear and nonclear days over IOP1 and IOP2, time of day (morning and afternoon), morning and afternoon over clear and nonclear days, and morning and afternoon over clear and nonclear days for IOP1 and IOP2 (Table 2). Clear days were first identified using MODIS *Aqua* and *Terra* cloud fractions of less than 20%. MODIS *Terra*'s orbit carries it south to north over the equator at approximately 1030 local time, and *Aqua* follows 3 h after at 1330 local time. Thus, there are 3 h between the two satellite observations, and they are

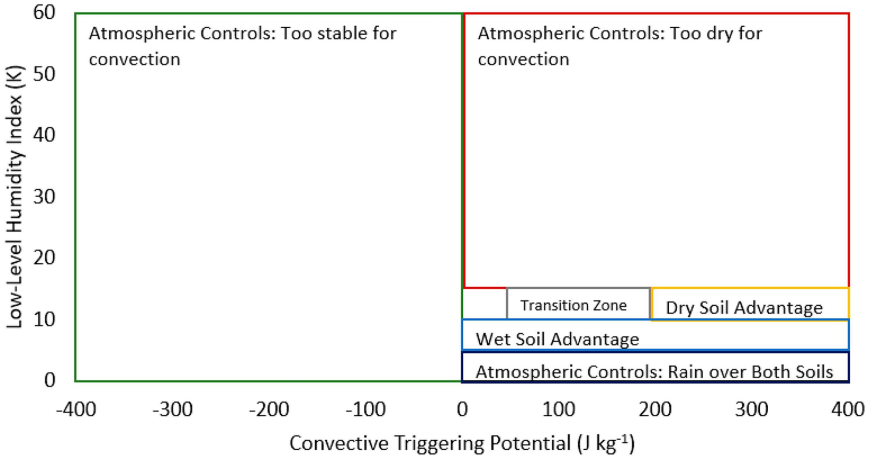

FIG. 2. CTP–HI_{low} framework categories (following Findell and Eltahir 2003a).

TABLE 2. Analysis and grouping of coupling metrics for different conditions to assess L–A interactions over irrigated and nonirrigated land uses.

Category	Additional description
IOP1 and IOP2	Regardless of cloud cover (clear vs nonclear days) and time of day (morning vs afternoon)
Cloud cover: clear vs nonclear days	Regardless of time of season (IOP1 and IOP2) and time of day (morning vs afternoon)
Cloud cover: clear vs nonclear days during IOP1 and IOP2	Regardless of time of day (morning vs afternoon)
Time of day	Regardless of time of season (IOP1 and IOP2) and cloud cover (clear vs nonclear days)
Time of day (morning vs afternoon) for IOP1 and IOP2	Regardless of cloud cover (clear vs nonclear days)
Time of day (morning vs afternoon) for clear vs nonclear days	Regardless of IOP1 and IOP2
Time of day (morning vs afternoon) for clear vs nonclear days during IOP1 and IOP2	

concentrated in the afternoon when the boundary layer is deepest. To ensure that other times during the day were consistently low-cloud cover, *GOES-16* satellite data from the NASA worldview (NASA 2021) were manually examined. When considering the shallow cumuli, the same threshold was applied, and days that produced deep convection were not counted as clear days. The rationale for including shallow cumuli despite potential shading effects is that they are indicative of a convectively active PBL, and restricting the cloud cover further leaves very few days upon which to conduct analysis. This methodology has been used successfully in other GRAINEX studies (e.g., Phillips et al. 2022).

After applying these criteria, we have found 5 clear days during IOP1 and 4 in IOP2 (total of 9 days). The remaining 21 days were classified as nonclear days. Statistical significance tests (t tests) were completed with a 95% confidence level. Subsequently, t tests were completed with a 90% confidence level to communicate additional important findings which did not meet the 95% confidence level requirement. Again, note that this study collected and analyzed a large amount of data, representing a wide variety of conditions through a large sampling of the atmosphere (1200 radiosonde launches in 30 days; 40 per day) so that the objectives of the experiment can be met.

3. Results

As noted previously, this paper aims to provide additional understanding of the impacts of irrigation on L–A interactions and the convective environment. Hence, analyses of coupling metrics were completed for IOP1 and IOP2 (section 3a) to determine whether periods of growing season alone can play an important role, regardless of time of day (morning vs afternoon) and sky condition (clear vs cloudy conditions) (Table 2). Note that typically afternoons are more favorable for convection development, while during clear skies irrigation can play an important role in L–A interactions (e.g., Rappin et al. 2021, 2022). Also, cloudy days could be linked to large-scale synoptic activities, which may dampen or mask L–A interactions. Furthermore, IOP1 and IOP2 represent the early and peak growing seasons, respectively, and during IOP2, irrigation becomes widespread.

Subsequently, an analysis of coupling metrics by clear versus cloudy days, regardless of IOP1 and IOP2, was used to determine whether irrigation forcing is sufficiently strong such that the growing period did not matter. Then, the three metrics were analyzed by clear versus cloudy days for IOP1 and IOP2 to determine whether growing periods along with background conditions provide an improved "signal" of land-use forcing (regardless of time of day) on L–A interactions and

TABLE 3. Mean CTP, HI_{low}, and LCL deficit (LCL–PBL) for IOP1, IOP2, clear days, and nonclear days. Statistical significance tests for the differences in means are completed for *irrigated* ISS3 vs *nonirrigated* ISS2, *irrigated* DOW8 vs *nonirrigated* ISS2, and *irrigated* ISS3 vs *transitional* DOW6. For brevity, significance tests were not completed for all possible combinations (e.g., ISS3 vs DOW7). Bold and italicized numbers represent those which have a $p < 0.05$ for the statistical significance test.

Site name	CTP (J kg^{-1})	HI_{low} (K)	LCL deficit (m)
	IOP1		
ISS2	115.27	20.77	***287.70***
ISS3	122.25	21.32	***417.13***
DOW6	115.72	20.66	***521.61***
DOW7	109.05	20.77	551.42
DOW8	110.25	20.89	***468.15***
	IOP2		
ISS2	76.78	***14.79***	101.44
ISS3	96.94	***11.41***	35.49
DOW6	75.52	***14.18***	102.05
DOW7	70.86	14.50	63.66
DOW8	68.65	***13.18***	60.70
	Clear		
ISS2	***50.34***	***22.82***	***203.93***
ISS3	***106.27***	***19.63***	***290.48***
DOW6	***67.97***	***21.70***	***405.87***
DOW7	70.17	21.97	427.19
DOW8	***73.21***	***20.10***	***312.60***
	Nonclear		
ISS2	115.61	15.62	191.63
ISS3	111.02	14.97	199.47
DOW6	108.82	15.56	271.45
DOW7	99.68	15.77	255.82
DOW8	97.62	15.77	245.18

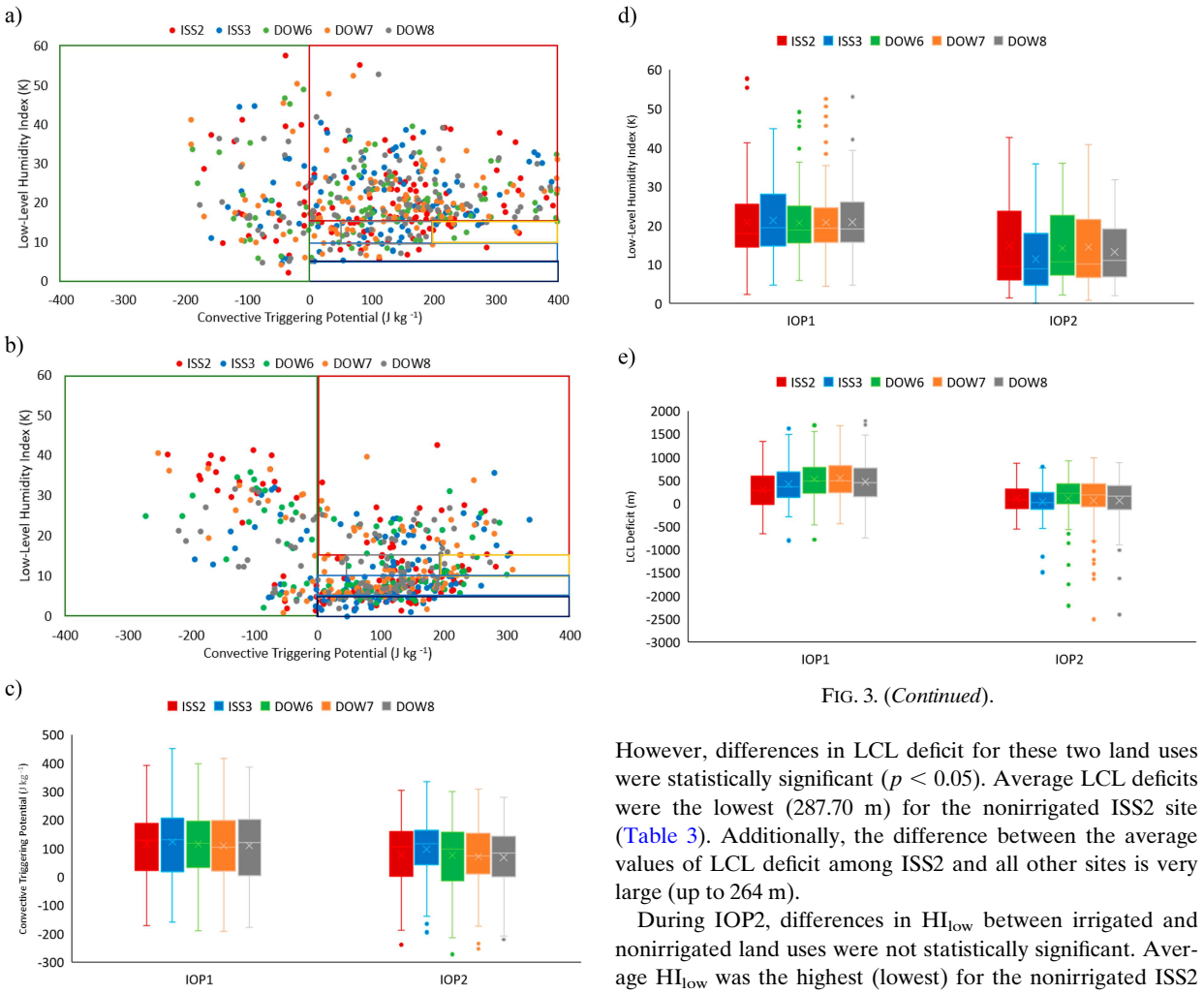

FIG. 3. Distributions of coupling metrics using scatterplots of CTP and HI_{low} for (a) IOP1 and (b) IOP2; box-and-whisker plots of (c) CTP, (d) HI_{low}, and (e) LCL deficit for IOP1 and IOP2. Dots and boxes with different colors represent radiosonde launching sites, which are identified at the top of each panel. ISS3 and DOW8 are irrigated locations, ISS2 and DOW7 are nonirrigated locations, and DOW6 is a transitional land-use zone (from irrigated to nonirrigated).

the convective environment. It is expected that clear days during IOP2 would provide the most noticeable response of the atmosphere to irrigation.

Coupling metrics subset by time of day (morning vs afternoon, regardless of IOP1 or IOP2); by time of day and IOP1 and IOP2; by time of day and clear versus cloudy conditions (regardless of IOP1 and IOP2); and by time of day, IOP1 and IOP2, and clear and cloudy conditions were also analyzed.

a. Early (IOP1) and peak (IOP2) growing seasons

Table 3 shows the mean statistics for CTP, HI_{low}, and LCL deficit for IOP1 and IOP2 and by clear and nonclear days. Differences in CTP and HI_{low} during IOP1 for irrigated and nonirrigated land uses were not statistically significant. However, differences in LCL deficit for these two land uses were statistically significant ($p < 0.05$). Average LCL deficits were the lowest (287.70 m) for the nonirrigated ISS2 site (Table 3). Additionally, the difference between the average values of LCL deficit among ISS2 and all other sites is very large (up to 264 m).

During IOP2, differences in HI_{low} between irrigated and nonirrigated land uses were not statistically significant. Average HI_{low} was the highest (lowest) for the nonirrigated ISS2 (irrigated ISS3) site at 11.41 K (14.79 K) (differences are statistically significant; $p < 0.05$). In other words, average HI_{low} for nonirrigated ISS2 was 0.29–3.38 K higher than the other sites (Table 3). Irrigated ISS3 (35.49 m) and DOW8 (60.70 m) show the two lowest LCL deficit values, while nonirrigated ISS2 shows the highest LCL deficit value (101.44 m). During IOP2, all sites demonstrate lower LCL deficit and HI_{low} values compared to IOP1. Irrigated ISS3 and irrigated DOW8 depict the largest decline forced by irrigation. Overall, irrigated ISS3 and DOW8 show more favorable conditions for convection than the nonirrigated areas, regardless of clear and nonclear conditions (benign vs nonbenign; Frye and Mote 2010) and time of day.

Figures 3a and 3b show the scatterplots of CTP and HI_{low} along with colored boxes depicting categories identified in Table 1 and Fig. 2. Most observations, regardless of location, were concentrated in the too dry for precipitation range (CTP $>$ 0 and $HI_{low} \geq 15$) during IOP1 (Fig. 3a). However, during IOP2, most observations were concentrated in the wet soil advantage (CTP $>$ 0 and $10 < HI_{low} < 15$). This change in the distribution of observations reflects the change in land surface conditions from IOP1 to IOP2. Given the lack of irrigation during the early growing season (IOP1) and widespread irrigation

during the peak growing season (IOP2), these results imply that irrigation is playing an important role in modifying the convective environment.

Figures 3c–e show the box-and-whisker plots of CTP, HI_{low}, and LCL deficit, respectively. The median CTP value for irrigated ISS3 during IOP2 was higher than the other sites. HI_{low} and LCL deficits show a noticeable lowering of their median values for irrigated ISS3 during IOP2, indicating the influence of irrigation. This result also suggests a moistening of the lower atmosphere linked to irrigated land use (Rappin et al. 2021, 2022; Phillips et al. 2022).

b. *Clear and nonclear days*

During clear days, average CTP was the highest (lowest) over irrigated ISS3 (nonirrigated ISS2) at 106.27 J kg^{-1} (50.34 J kg^{-1}) (Table 3). In other words, average CTP for irrigated ISS3 was 33.06–55.93 J kg^{-1} higher than the other sites. Average HI_{low} was the lowest (highest) over irrigated ISS3 (nonirrigated ISS2) at 19.62 K (22.82 K). Thus, average HI_{low} over irrigated ISS3 was 0.43–3.2 K lower than the other sites (Table 3). Average LCL deficits were the lowest (highest) over the nonirrigated ISS2 (DOW7) site at 203.93 m (427.19 m). Hence, average LCL deficits at ISS2 are 86.55–223.36 m lower than the other sites (Table 3).

Although differences in CTP, HI_{low}, and LCL deficit between irrigated and nonirrigated sites for nonclear days were not statistically significant, we found an average increase in CTP and lowering of HI_{low} and LCL deficit values for all sites. Based on the observations, it is difficult to discern the influence of the land surface simply based on the large-scale atmospheric setup. In other words, it is important to conduct an analysis that also incorporates land surface conditions such as early (IOP1) versus peak (IOP2) growing seasons, which captures the extent of the crop/vegetation cover and status of irrigation/soil moisture.

c. *Clear and nonclear days during early (IOP1) and peak (IOP2) growing seasons*

To further understand irrigation impacts, an analysis using coupling metrics for clear and nonclear days over IOP1 and IOP2 was completed. Table 4 shows the mean values of CTP, HI_{low}, and LCL deficit along with the results of the statistical significance testing. During clear days in IOP1, differences in CTP between irrigated and nonirrigated land uses were statistically not significant. Average HI_{low} during clear days in IOP1 was the highest (lowest) for the irrigated ISS3 (nonirrigated ISS2) site at 19.61 K (16.54 K). In other words, irrigated ISS3 has average HI_{low} values that are 0.77–3.07 K higher than the other sites (Table 4). Average LCL deficits during clear days in IOP1 were the highest (lowest) for the nonirrigated DOW7 (nonirrigated ISS2) site at 435.98 m (157.44 m). Average LCL deficits for the nonirrigated DOW7 site are 8.7–287.24 m higher than the other sites (Table 4). Overall, based on LCL deficit and HI_{low}, the nonirrigated land shows slightly more favorability toward convective development.

During clear days in IOP2, average CTP was the highest (lowest) for the irrigated ISS3 (nonirrigated ISS2) site at 76.99 J kg^{-1} (−28.75 J kg^{-1}). Moreover, CTP at ISS3 during IOP2 was 55.09–105.74 J kg^{-1} higher than the other sites (Table 4). Average HI_{low} was the highest (lowest) for the nonirrigated ISS2 (irrigated ISS3) site at 30.68 K (19.66 K). Average LCL deficit was the highest (lowest) for the nonirrigated DOW7 (irrigated ISS3) site at 405.96 m (180.46 m) and was 36.66–225.5 m higher than the other sites (Table 4). These results suggest that, compared to nonirrigated land use, irrigated land use increased convective potential during IOP2 when irrigation applications increased due to increases in crop water demand.

Average LCL deficits during nonclear days in IOP1 were the lowest for DOW7, a nonirrigated site, at 607.26 m and were 40.86–251.41 m higher than the other sites (Table 4). For IOP2, this condition reversed for DOW7, which showed the lowest average LCL deficit. However, if we consider results from CTP, HI_{low}, and LCL deficit (differences are not statistically significant) for the two most well-representative irrigated (ISS3) and nonirrigated (ISS2) sites, then during nonclear days in IOP2 conditions were comparatively more favorable for convection development over irrigated land use. In short, if land-use forcing is sufficiently large, it does not matter whether background atmospheric conditions are "benign" or "nonbenign" (e.g., Frye and Mote 2010), and its impacts on the convective environment are discernible.

TABLE 4. Mean CTP, HI_{low}, and the LCL deficit (LCL–PBL) for clear and nonclear days during IOP1 and IOP2. Statistical significance tests for the differences in means are completed for *irrigated* ISS3 vs *nonirrigated* ISS2, *irrigated* DOW8 vs ISS2, and *irrigated* ISS3 vs *transitional* DOW6. For brevity, significance tests were not completed for all possible combinations (e.g., ISS3 vs DOW7). Bold values represent those which have a $p < 0.1$ in t tests, while bold and italicized values represent those which have a $p < 0.05$.

Site name	CTP (J kg^{-1})	HI_{low} (K)	LCL deficit (m)
	Clear IOP1		
ISS2	113.61	***16.54***	***157.44***
ISS3	129.69	***19.61***	***381.09***
DOW6	119.01	***18.30***	***435.98***
DOW7	108.78	***18.11***	444.68
DOW8	117.98	***18.84***	***325.43***
	Clear IOP2		
ISS2	***−28.75***	***30.68***	**260.39**
ISS3	***76.99***	***19.66***	**180.46**
DOW6	***5.98***	***25.83***	**369.3**
DOW7	***21.90***	***26.79***	405.96
DOW8	***17.24***	***21.69***	**297.01**
	Nonclear IOP1		
ISS2	116.11	22.89	***355.85***
ISS3	118.53	22.18	***435.98***
DOW6	114.05	21.86	***566.4***
DOW7	109.19	22.14	607.26
DOW8	106.27	21.95	***542.81***
	Nonclear IOP2		
ISS2	115.16	9.02	36.94
ISS3	104.20	8.41	−23.33
DOW6	103.74	9.45	−6.39
DOW7	90.45	9.59	−75.24
DOW8	89.22	9.77	−35.2

Figures 4a–c show the box-and-whisker plots of CTP, HI_{low}, and LCL deficits for all sites by cloud cover and IOP. For clear days in IOP1, median values of CTP were the highest (slightly <200 J kg^{-1}) for the nonirrigated ISS2 location (Fig. 4a). Median values of HI_{low} were the lowest ($10 < HI_{low} < 15$) for the nonirrigated ISS2 site. Together, they indicate a transition zone (Table 1) for convection, which is expected for nonirrigated land use during IOP1 when the land surface was sufficiently and naturally wet (to support the rainfed crop) in the eastern part of the study area (Fig. 4b). Median values of LCL deficits during clear days in IOP1 were the highest (lowest) for the transitional land-use DOW6 (nonirrigated ISS2) site. Negative skewness was noted for the transitional land-use DOW6 and irrigated DOW8 sites. In other words, above-average values of LCL deficit appeared more frequently at these sites (Fig. 4c).

For clear days in IOP2, median values for CTP were the highest (lowest) for the irrigated ISS3 (nonirrigated ISS2) site (Fig. 4a). Negative skew was noticed for the nonirrigated ISS2, irrigated ISS3, and irrigated DOW8 sites (Fig. 3a). Median values of HI_{low} during clear days in IOP2 were the lowest (~19 K) (highest; ~30 K) for the irrigated ISS3 (nonirrigated ISS2) site (Fig. 4b). Median values of LCL deficits were the lowest for the irrigated ISS3 site (Fig. 4c). Together, these metrics demonstrate that irrigated land use favorably impacted the convective environment on clear days. These changes are most visible for ISS3 (irrigated land use) and ISS2 (nonirrigated land use).

For nonclear days in IOP1, the median value of CTP was the highest (lowest) for the nonirrigated ISS2 (nonirrigated DOW7) site. A slight positive skew was noted for irrigated ISS3, transitional land-use DOW6, and nonirrigated DOW7 sites (Fig. 4a). Median values of HI_{low} were the highest (lowest) for the irrigated ISS3 (nonirrigated ISS2) site (Fig. 4b). Median values of LCL deficit during nonclear days in IOP1 were the highest (lowest) for the nonirrigated DOW7 (nonirrigated ISS2) site (Fig. 4c). For nonclear days in IOP2, median values of CTP were the highest (lowest) for the irrigated ISS3 (nonirrigated DOW7) site. The lowest median values of HI_{low} and LCL deficit were found for irrigated ISS3. There was a clear shift toward lower HI_{low} and LCL deficit values during IOP2 under nonclear days across all sites with the most noticeable changes over irrigated land use (ISS3) (Table 4). Again, these suggest irrigation forcing on the convective environment.

d. *Time of day (morning vs afternoon)*

CTP, HI_{low}, and LCL deficit were calculated by time of day to investigate whether time of day has an influence on L–A coupling. First, we analyzed the data based on time of day *without* considering land use and period of the season [early growing season (IOP1) vs peak growing season (IOP2)] (Figs. 5a–e). As noted previously, soundings launched from 1300 to 1700 UTC were considered morning soundings, while soundings launched from 1900 to 0100 UTC were considered afternoon soundings. Figures 5a–e show the distributions of coupling metrics by time of day, with Figs. 5a and 5b showing the scatterplots of CTP and HI_{low} for morning and afternoon and Figs. 5c–e

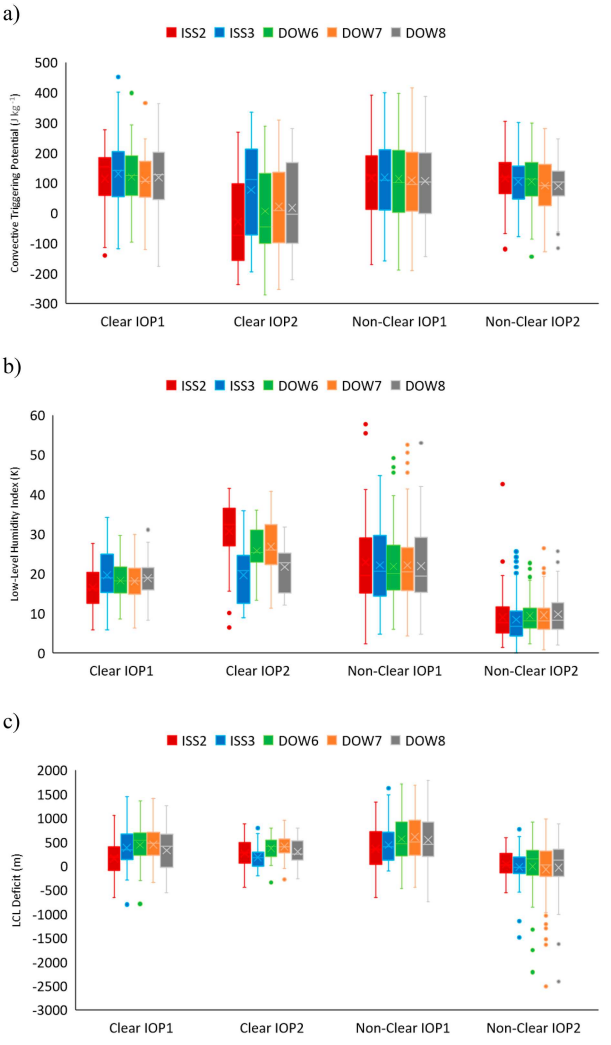

FIG. 4. Box-and-whisker plots of (a) CTP, (b) HI_{low}, and (c) LCL deficit by cloud cover and IOP. Boxes with different colors represent different radiosonde launching sites, which are identified at the top of each panel. ISS3 and DOW8 are irrigated locations, ISS2 and DOW7 are nonirrigated locations, and DOW6 is a transitional land-use zone (from irrigated to nonirrigated).

showing the box-and-whisker plots of CTP, HI_{low}, and LCL deficits. For both mornings and afternoons, overall differences in CTP, HI_{low}, and LCL deficit were not statistically significant. However, the distribution for the morning is more scattered, while the afternoon data are concentrated at higher values signifying more mixing in the boundary layer atmosphere.

e. *Time of day and early IOP1 and peak (IOP2) growing seasons*

To further understand L–A interactions, the coupling metrics were analyzed by time of day and IOP1 and IOP2. Table 4 shows the mean values of CTP, HI_{low}, and LCL deficit. For mornings in IOP1, differences in CTP and HI_{low} for irrigated and nonirrigated land uses were statistically not significant.

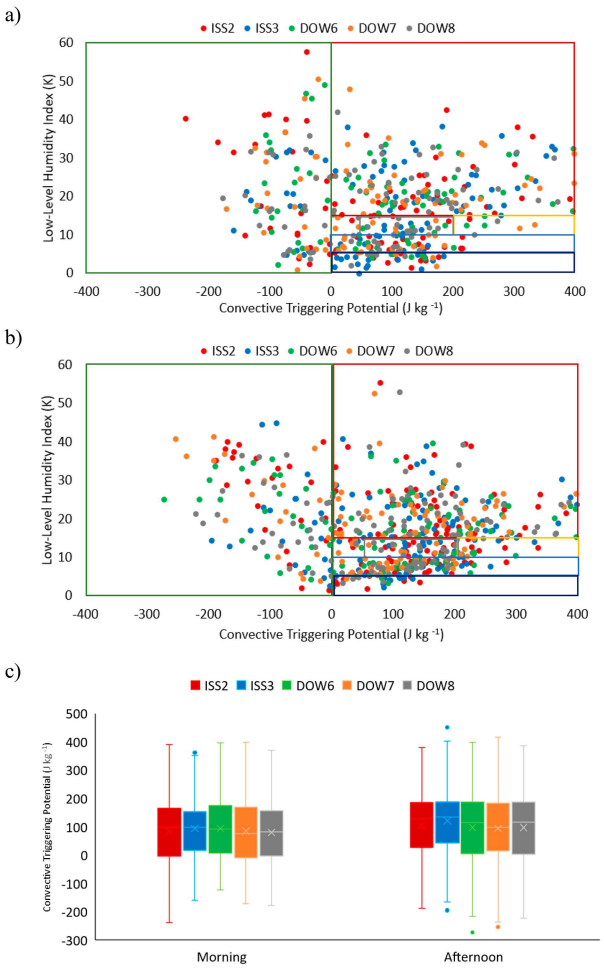

FIG. 5. Scatterplots of CTP and HI_{low} for (a) morning and (b) afternoon; and box-and-whisker plots of (c) CTP, (d) HI_{low}, and (e) LCL deficit. Dots and boxes with different colors represent radiosonde launching sites, which are identified at the top of each panel. ISS3 and DOW8 are irrigated locations, ISS2 and DOW7 are nonirrigated locations, and DOW6 is a transitional land-use zone (from irrigated to nonirrigated).

However, differences in LCL deficit between irrigated and nonirrigated land uses were statistically significant ($p < 0.05$) (Table 5). Average LCL deficits during the mornings of IOP1 were the highest (lowest) for the nonirrigated DOW7 (nonirrigated ISS2) site at 617.78 m (393.41 m). In other words, DOW7 had average LCL deficits that are 45.32–224.37 m higher than the other sites (Table 4). Due to the drier condition and hence more sensible heat flux over nonirrigated DOW7, both PBL and LCL heights increase, resulting in higher LCL deficits (cf. Fig. 10; Rappin et al. 2021).

For mornings in IOP2, differences in CTP between the two land uses were not statistically significant. Average HI_{low} during mornings in IOP2 was the highest (lowest) for the transitional land-use DOW6 (irrigated ISS3) site at 14.77 K (11.64 K) (Table 5). The lowest HI_{low} value is linked to the irrigated ISS3, while the highest HI_{low} value is linked to the transitional

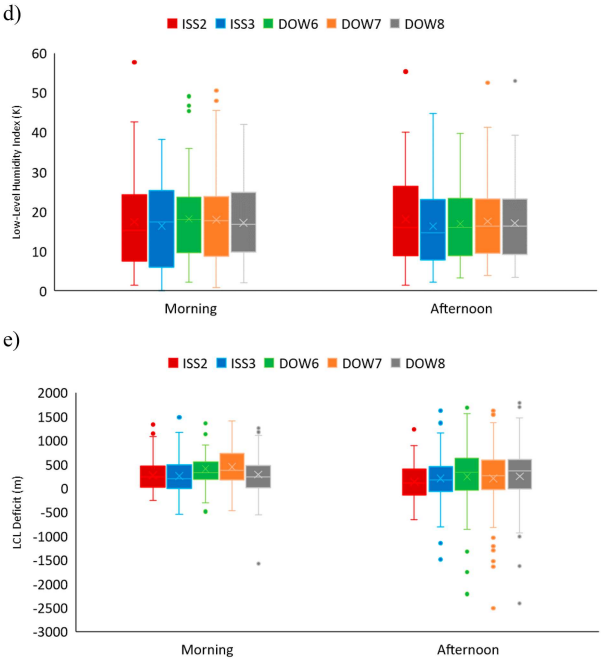

FIG. 5. (*Continued*).

land-use DOW6 location, suggesting impacts of land-use and surface moistness. The differences in HI_{low} between irrigated ISS3 and transitional land-use DOW6 were statistically significant ($p < 0.1$). Average LCL deficits during mornings of IOP2 were the highest (lowest) for the nonirrigated DOW7 (irrigated ISS3) site at 262.46 m (68.60 m). In other words, average LCL deficits for the nonirrigated DOW7 site were 32.76–193.86 m higher than all other sites. Also, the second lowest LCL deficit value (85.18 m) was observed for irrigated DOW8. The differences in LCL deficits between irrigated and nonirrigated land uses were statistically significant ($p < 0.1$). These low LCL deficit and HI_{low} coupling metrics are an indication of irrigation's impact.

For afternoons in IOP1, differences in CTP, HI_{low}, and LCL deficit between irrigated and nonirrigated locations were not statistically significant. The same applies for CTP and LCL deficit in IOP2, while HI_{low} shows a statistically significant difference ($p < 0.05$) (Table 5). Further, LCL deficit is noticeably lower during afternoons of IOP2 for all locations than in the mornings of IOP1 and IOP2. Additionally, during IOP2, CTP and HI_{low} were indicating a wet soil advantage for irrigated ISS3 and irrigated DOW8 locations. It is observed that, compared to IOP1 HI_{low} (>20 K), IOP2 HI_{low} was lower (11.23–14.84 K) during the afternoons. Overall, it was found that convective favorability increased for all sites during IOP2, with irrigated land use providing higher favorability, regardless of cloud conditions (clear or nonclear) (Table 5).

Figures 6a–c show the box-and-whisker plots of CTP, HI_{low}, and LCL deficit by time of day and IOP. Based on the LCL deficit and HI_{low} values, it is evident that afternoons of IOP2 were more favorable for convection development, which agrees with the previous assessment linked to Table 5.

TABLE 5. Mean CTP, HI_{low}, and the LCL deficit (LCL–PBL) for morning and afternoon of IOP1 and IOP2. Statistical significance tests for the differences in means are completed for *irrigated* ISS3 vs *nonirrigated* ISS2, *irrigated* DOW8 vs ISS2, and *irrigated* ISS3 vs *transitional* DOW6. For brevity, significance tests were not completed for all possible combinations (e.g., ISS3 vs DOW7). Bold values represent those which have a $p < 0.1$ in *t* tests, while bold and italicized values represent those which have a $p < 0.05$.

Site name	CTP (J kg^{-1})	HI_{low} (K)	LCL deficit (m)
	Morning IOP1		
ISS2	95.19	20.07	**393.41**
ISS3	101.45	21.22	**439.25**
DOW6	115.30	21.41	**572.46**
DOW7	102.25	21.16	617.78
DOW8	91.00	20.48	**484.78**
	Morning IOP2		
ISS2	72.62	**14.73**	**142.00**
ISS3	86.31	**11.64**	**68.60**
DOW6	72.36	**14.77**	**229.70**
DOW7	66.22	14.49	262.46
DOW8	67.83	**13.66**	**85.18**
	Afternoon IOP1		
ISS2	130.34	21.29	203.15
ISS3	137.85	21.40	399.44
DOW6	116.05	20.09	480.93
DOW7	114.32	20.47	498.34
DOW8	125.18	21.21	454.85
	Afternoon IOP2		
ISS2	79.91	***14.84***	70.47
ISS3	104.91	***11.23***	10.22
DOW6	77.93	***13.72***	4.58
DOW7	74.34	***14.51***	−88.16
DOW8	69.27	***12.81***	41.99

f. Time of day and cloud cover (clear vs nonclear days)

Table 5 shows the average values of CTP, HI_{low}, and LCL deficit regardless of IOPs. For clear mornings, the average CTP was the highest (lowest) for irrigated ISS3 (nonirrigated ISS2) site at 71.41 J kg^{-1} (16.77 J kg^{-1}) (Table 6). The highest (lowest) HI_{low} value was 21 K (19.60 K) for transitional land-use DOW6 (irrigated DOW8) site. The largest (lowest) LCL deficit was 430.48 m (242.32 m) for transitional land-use DOW6 (irrigated DOW8) site. DOW8 was located over an irrigated area, and coupling metrics indicate the influence of irrigated land use. Differences in HI_{low} and LCL deficits for irrigated and nonirrigated land uses during clear mornings were statistically not significant.

Average CTP during clear afternoons is the highest (lowest) for the irrigated ISS3 (nonirrigated ISS2) site at 132.40 J kg^{-1} (75.51 J kg^{-1}) (Table 1 in the online supplemental material). In addition, average HI_{low} during clear afternoons is the highest (lowest) for the nonirrigated ISS2 (irrigated ISS3) site at 24.43 K (19.39 K) (supplemental Table 1). The difference in CTP and HI_{low} values between irrigated and nonirrigated land uses and clear afternoons is statistically significant ($p < 0.05$). For nonclear mornings, differences in CTP and HI_{low} over the two land uses were not statistically significant. For nonclear mornings, the average LCL deficit was the highest (lowest) for the nonirrigated DOW7 (irrigated ISS3) site at 451.65 m (234.38 m). Based on the CTP, HI_{low}, and LCL deficit, compared to nonclear mornings, it appears that nonclear afternoons are more favorable for convective development for all land-use types during GRAINEX (supplemental Table 1).

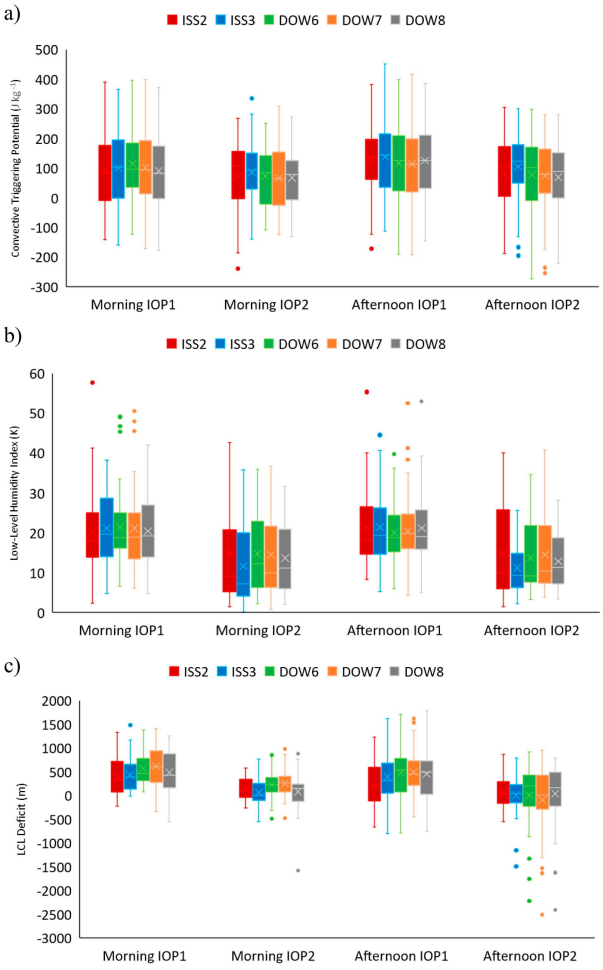

FIG. 6. Box-and-whisker plots of (a) CTP, (b) HI_{low}, and (c) LCL deficit by time of day and IOP. Boxes with different colors represent radiosonde launching sites, which are identified at the top of each panel. ISS3 and DOW8 are irrigated locations, ISS2 and DOW7 are nonirrigated locations, and DOW6 is a transitional land-use zone (from irrigated to nonirrigated).

Supplemental Figs. 1a–c show the box-and-whisker plots of CTP, HI_{low}, and LCL deficits by cloud cover and time of day. Again, compared to clear mornings, CTP values tend to be higher during clear afternoons. Irrigated ISS3 shows the most noticeable CTP and HI_{low} changes from morning to afternoon. For clear mornings, median values of CTP were the highest (lowest) for the ISS3 (ISS2) site.

g. Time of day and cloud cover during early (IOP1) and peak (IOP2) growing seasons

To further understand the influence of irrigation and land use, we assessed coupling metrics for clear mornings of IOP1 and IOP2, clear afternoons of IOP1 and IOP2, nonclear

TABLE 6. Mean CTP, HI_{low}, and LCL deficit (LCL–PBL) for clear morning of IOP1 and IOP2, clear afternoon of IOP1 and IOP2, nonclear morning of IOP1 and IOP2, and nonclear afternoon of IOP1 and IOP2. Statistical significance tests for the differences in means are completed for *irrigated* ISS3 vs *nonirrigated* ISS2, *irrigated* DOW8 vs ISS2, and *irrigated* ISS3 vs *transitional* DOW6. For brevity, significance tests were not completed for all possible combinations (e.g., ISS3 vs DOW7). Bold values represent those which have a $p \leq 0.1$ in t tests, while bold and italicized values represent those which have a $p \leq 0.05$.

Site name	CTP (J kg^{-1})	HI_{low} (K)	LCL deficit (m)	Site name	CTP (J kg^{-1})	HI_{low} (K)	LCL deficit (m)
	Clear morning IOP1				Clear morning IOP2		
ISS2	54.33	***13.94***	284.71	ISS2	**−30.18**	29.10	254.33
ISS3	55.69	***17.96***	429.43	ISS3	**91.07**	22.43	177.75
DOW6	55.26	***16.49***	509.46	DOW6	**21.57**	26.27	338.34
DOW7	48.75	15.25	458.92	DOW7	23.80	27.23	390.13
DOW8	47.42	***16.75***	325.27	DOW8	**38.67**	23.17	145.53
	Clear afternoon IOP1				Clear afternoon IOP2		
ISS2	158.06	18.48	68.35	ISS2	**−27.68**	***31.86***	264.94
ISS3	185.19	20.84	347.25	ISS3	**66.42**	***17.58***	182.5
DOW6	163.64	19.56	384.55	DOW6	**−5.72**	***25.50***	392.52
DOW7	153.80	20.25	434.71	DOW7	20.48	26.46	417.84
DOW8	170.90	20.40	325.55	DOW8	**1.16**	***20.58***	410.62
	Nonclear morning IOP1				Nonclear morning IOP2		
ISS2	115.62	23.14	***444.13***	ISS2	110.00	9.51	91.07
ISS3	124.34	22.85	***443.83***	ISS3	84.58	7.72	24.93
DOW6	143.31	23.70	***601.86***	DOW6	92.68	10.18	186.25
DOW7	129.00	24.12	691.91	DOW7	83.19	9.40	211.40
DOW8	112.79	22.34	***559.22***	DOW8	79.49	9.86	61.05
	Nonclear afternoon IOP1				Nonclear afternoon IOP2		
ISS2	116.47	22.70	280.17	ISS2	119.03	**8.65**	−9.31
ISS3	114.18	21.68	429.26	ISS3	118.91	**8.92**	−60.46
DOW6	90.32	20.37	536.00	DOW6	112.25	**8.89**	−154.58
DOW7	93.55	20.59	534.71	DOW7	95.89	9.73	−295.74
DOW8	101.12	21.64	528.74	DOW8	96.52	**9.71**	−109.24

mornings of IOP1 and IOP2, and nonclear afternoons of IOP1 and IOP2. On clear days when land-use forcing is expected to be higher, it is found that LCL deficit was the lowest (182.5 m) in the afternoon over irrigated areas (ISS3) during IOP2 (Table 6). It is also found that CTP (66.42 J kg^{-1}) and HI_{low} (17.58 K) were the highest and the lowest, respectively, over irrigated land use (ISS3) than the other locations in the afternoon during IOP2 (Table 6). The difference between irrigated and nonirrigated land uses for CTP and HI_{low} was statistically significant. Similar results were found during IOP2 clear mornings; however, the difference between irrigated and nonirrigated land uses is not statistically significant. These results are further shown in Figs. 7a–c.

For nonclear days of IOP1 and IOP2 when larger-scale influences were prominent, land-use influence on the atmosphere and its convective environment was not as clear. However, both the afternoon and mornings of IOP2 show clearer land-use influence via lower HI_{low} and LCL deficit and relatively higher CTP. Further assessment shows that the second lowest HI_{low} and the second highest CTP during the afternoon hours of IOP2 occurred over irrigated areas, coincident with a negative LCL deficit, suggesting favorable conditions for cloud development. Hence, irrigation impacts are discernible even when a large-scale atmospheric influence is present.

A further summary of the results is presented in Figs. 8a–l with a focus on IOP2 when irrigation impacts are most prominent. The CTP and HI_{low} values and observed data from the three DOW sites were used and supplemented by two nearby National Weather Service operated radars (the KOAX and KUEX; National Centers for Environmental Information 2022). These data were used to determine whether convection was possible and identify the observed convection. Data were aggregated under three categories: no convection possible (NCP), convection observed (CO), and convection possible but not observed (CPNO). When a CTP value was negative and/or a HI_{low} value was 15 or higher, it was concluded that conditions were not favorable for convection. In other words, the atmosphere was either too dry or too stable for precipitation to occur (Table 1). When a CTP and HI_{low} value fulfilled any of the other categories, but there was no convection observed from a 2-h span between soundings, then it was identified that convection was possible, but not observed (CPNO). Otherwise, there was observed convection (CO).

Overall (without separating the data between clear and nonclear days and between morning and afternoon), it is found that, compared to nonirrigated land use, total CO was only 1% higher over irrigated areas during IOP2 (Figs. 8a,b). However, compared to nonirrigated land use, CPNO observations were 4% higher over irrigated land use (Figs. 8a,b). In addition, when we separate the data by clear and nonclear days, we have found that CPNO was 28% higher over irrigated areas (Figs. 8c,d).

On the other hand, when coupling metrics and radar observations were assessed for all mornings, the frequency of CO and CPNO was 4% higher while that of NCP was 9% lower for irrigated land use (Figs. 8e,f). Thus, in this case, irrigated

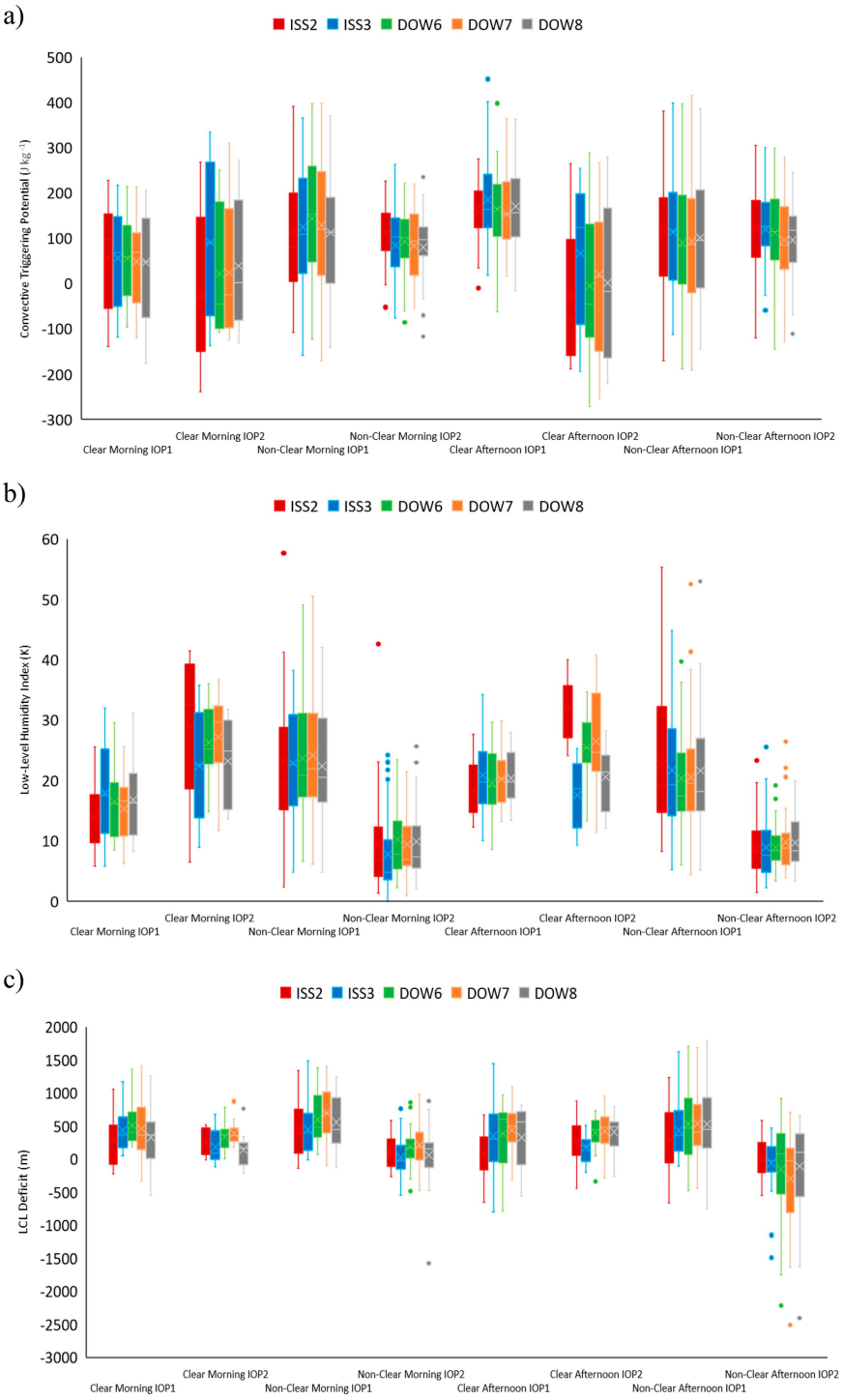

FIG. 7. Box-and-whisker plots of (a) CTP, (b) HI_{low}, and (c) LCL deficit by IOP, cloud cover, and time of day. Boxes with different colors represent radiosonde launching sites, which are identified at the top of each panel. ISS3 and DOW8 are irrigated locations, ISS2 and DOW7 are nonirrigated locations, and DOW6 is a transitional land-use zone (from irrigated to nonirrigated).

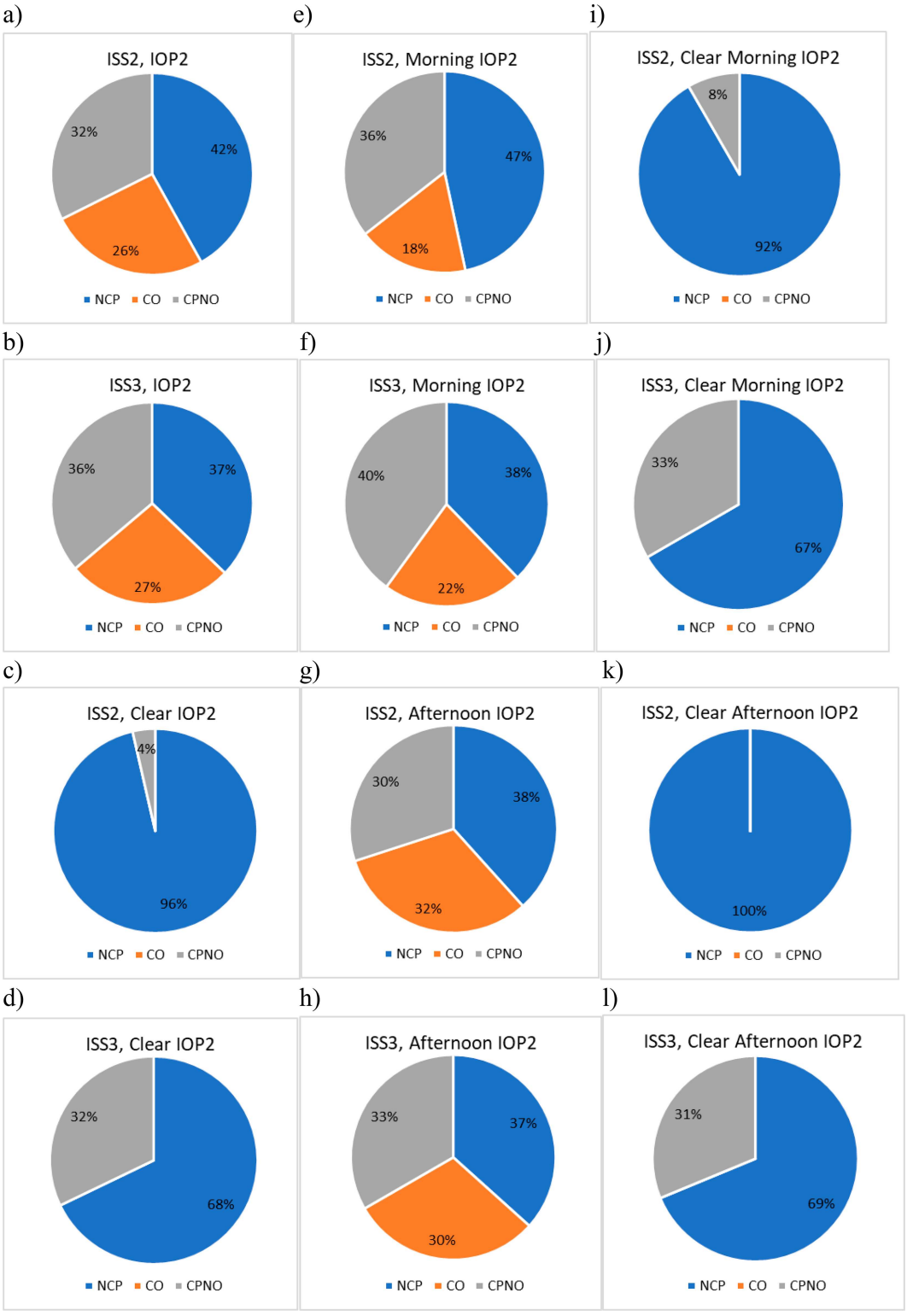

FIG. 8. Convective possibilities for (a) ISS2, IOP2; (b) ISS3, IOP2; (c) ISS2, clear IOP2; (d) ISS3, clear IOP2; (e) ISS2, morning IOP2; (f) ISS3, morning IOP2; (g) ISS2, afternoon IOP2; (h) ISS3, afternoon IOP2; (i) ISS2, clear morning IOP2; (j) ISS3, clear morning IOP2; (k) ISS2, clear afternoon IOP2; and (l) ISS3, clear afternoon IOP2. NCP is no convection possible, CO is convection observed, and CPNO is convection possible but not observed. ISS3 and ISS2 are *irrigated* and *nonirrigated* locations, respectively.

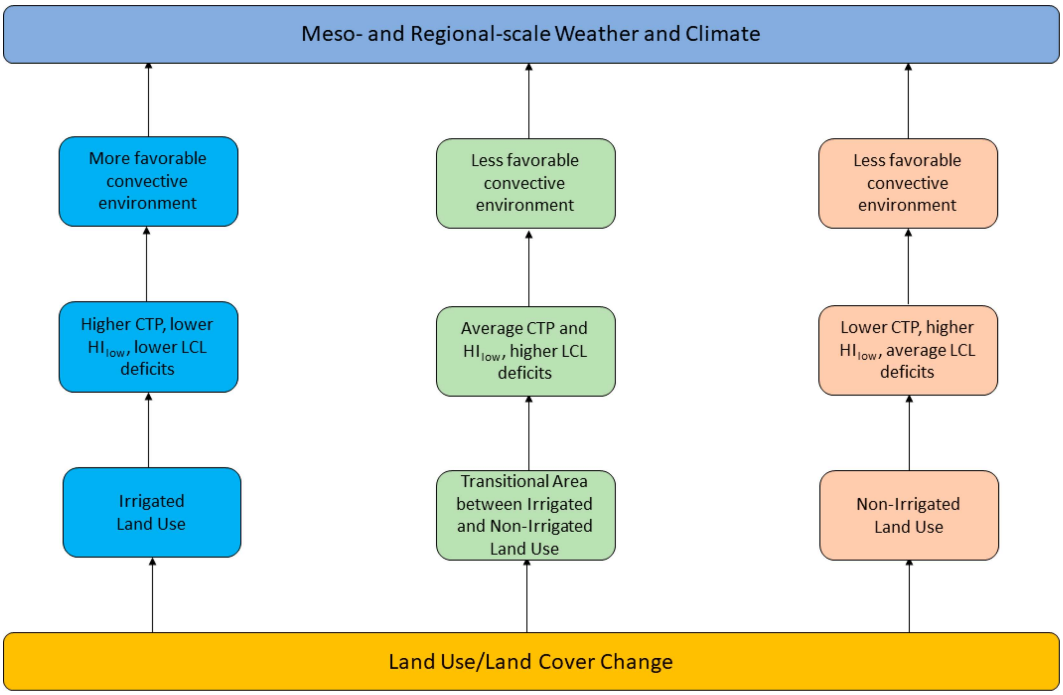

FIG. 9. Summary of the impacts of LULCC on L–A coupling metrics and convective outcomes.

land use favors convection. For all afternoons (not separating between clear and nonclear days), irrigated land use favors convection slightly more (CO + CPNO) than nonirrigated land use (Figs. 8g,h). However, when we assess observations from clear mornings, the frequency of CPNO was 25% higher over irrigated areas (Figs. 9i,j), while it was 31% higher during afternoons (Figs. 8k,l). Hence, irrigated land use was favoring convective development during clear conditions, regardless of morning or afternoon.

4. Discussion

L–A interactions are complex. Irrigated LULCC and the resultant increase in soil moisture add further intricacies to this relationship. The unique GRAINEX dataset allowed us, for the first time, to investigate L–A interactions over irrigated and nonirrigated conditions side by side and for different atmospheric conditions (clear vs cloudy, with the latter sometimes under larger-scale synoptic and advective influences), different periods of the growing season, and throughout the day (e.g., morning vs afternoon). Irrigation, and the resultant increase in soil moisture, creates a wet soil advantage and favors wet coupling due to modified heat flux partitioning and via L–A feedback (Roundy and Santanello 2017).

This paper quantified L–A interactions under a wide variety of conditions using a framework developed by Findell and Eltahir (2003a,b) and the formulation modified by Ferguson and Wood (2011). A key advantage of this study is that it used radiosonde data collected throughout the day (eight observations per day) as opposed to only morning data (one observation per day) used by Findell and Eltahir (2003a,b). Hence, the data collected during GRAINEX allowed us to expand on Findell and Eltahir (2003a,b) and investigate L–A interactions and irrigation's influence during the latter part of the day (e.g., afternoon) when convection typically develops.

However, it should be noted that the CTP methodology of Findell and Eltahir (2003a,b) was developed with morning soundings in mind, in which the effect of the residual thermodynamic structure from the previous night is included. While the morning CTP can still be interpreted using the theoretical framework developed by Findell and Eltahir (2003a), the CTP from the afternoon soundings is different given that the boundary layer has already developed at that point. CTP during the afternoon still represents the same physical quantity as the morning CTP; however, the interpretation of the value is different given that CTP is no longer representative of the residual boundary layer's properties, but rather of the developed boundary layer of that day. So, rather than looking at CTP as representing the potential for convection later in the day, it is representative of how the boundary layer developed through the day (toward a dry adiabatic profile in the case of larger CTP values compared to the morning or maintaining a moist adiabatic profile in the case of smaller afternoon CTP values). Thus, the afternoon CTP aids in the identification of when sensible (in the case of larger afternoon CTP values) or latent (in the case of smaller afternoon CTP values) heat fluxes are driving boundary layer property changes throughout the day.

It is well known that favorable conditions for convective development (and precipitation) can occur due to 1) advection of moisture linked to large-scale circulation, 2) utilization of moisture linked to local sources including land use (irrigation

in this case), and 3) a combination of both. It is also possible that the large-scale influence dominates and overshadows/suppresses local (e.g., land use/irrigation) influences on low-level atmospheric development and any resultant precipitation. In this study, it was found that irrigation's influence can be sufficiently large so that it provides favorable environment for convection and cloud development under a variety of conditions.

Results suggest that, with a few exceptions, the transition from the early growing season (early June/early summer) to the peak growing season (late July/peak summer) leads to a decline in CTP, HI_{low}, and LCL deficits. In other words, as we moved from IOP1 to IOP2, average CTP, HI_{low}, and LCL deficits all decreased. Although CTP declined, it was well above zero in all cases. As a result, the CTP values during IOP2, along with lower HI_{low} and LCL deficit, offered overall favorable conditions for convection. Additionally, with the transition from the early summer (IOP1) to the peak summer (IOP2) and increased irrigation, conditions became more favorable for convective development over irrigated land use. Note that ISS2 and ISS3 are located over nonirrigated and irrigated land uses, respectively. The DOW sites are located in the irrigated (DOW8), nonirrigated (DOW7), and boundary between irrigated and nonirrigated land uses (transitional) (DOW6). LCL deficits during IOP1 were the lowest for nonirrigated land use and the highest for the transition zone between irrigated and nonirrigated land uses. During IOP1, naturally occurring soil moisture was higher over nonirrigated land use (e.g., Fig. 3c, Rappin et al. 2021), which supports rainfed agriculture. This also leads to higher ET and results in a lower LCL deficit. On the other hand, for IOP2, HI_{low} values for irrigated ISS3 were the lowest of all the sites. This suggests that the increase in moisture due to irrigation resulted in lower HI_{low} for the ISS3 site than all other sites. Thus, land use impacted the convective environment with the effect further evident during IOP2 when irrigation is widespread (e.g., Fig. 3c; Rappin et al. 2021).

After aggregating the metrics by IOPs, LCL deficit and HI_{low} show a statistically significant difference between irrigated and nonirrigated land uses for clear days during IOP1 and IOP2. Similar results were found for CTP but only during IOP2. Clear days in IOP1 observed higher HI_{low} over irrigated land use than the other sites. Additionally, over irrigated land use, LCL deficits were higher than nonirrigated land use. This changed with clear days in IOP2 where HI_{low} and LCL deficits were lower over irrigated land use than nonirrigated land use. For nonclear days in IOP1 and IOP2, differences in CTP and HI_{low} were not statistically significant between irrigated and nonirrigated land uses. However, LCL deficits showed statistically significant differences during nonclear days in IOP1, with irrigated land use reporting lower LCL deficits than nonirrigated cropland. These results were impacted by the presence of synoptic forcing causing similarities in the results.

Analyzing the metrics by day with and without cloud cover (i.e., clear vs nonclear) allows for an understanding of cloud cover impacts on CTP, HI_{low}, and LCL deficits in the context of land use (irrigated vs nonirrigated). Note that cloud cover can indicate the presence of large-scale synoptic influence. It is found that during cloudy days (regardless of time of the growing season; i.e., IOP1 or IOP2), differences in CTP, HI_{low}, and LCL deficits over irrigated versus nonirrigated land uses are statistically not significant. On the other hand, for clear days, differences in CTP, HI_{low}, and LCL deficits over irrigated and nonirrigated land uses are statistically significant. The CTP and HI_{low} values for the transitional land-use area were generally in between, compared to values from irrigated and nonirrigated areas.

Aggregating and analyzing the metrics by time of day shows increases in CTP for the ISS sites from morning to afternoon. These changes were not observed in the DOW sites. Changes in HI_{low} from morning to afternoon were negligible for all sites. As expected, LCL deficits decreased from morning to afternoon with the diurnal cycle enhancing mixing, and thus, PBLH increased and the LCL deficit decreased.

Analyzing the data by time of day and IOP, it was found that the difference in morning CTP values between irrigated and nonirrigated land uses was not statistically significant for IOP1 and IOP2. However, differences in LCL deficit between irrigated and nonirrigated land uses for IOP1 and IOP2 mornings were statistically significant. LCL deficits during mornings in IOP1 (IOP2) were the lowest for nonirrigated (irrigated) land use. The LCL deficit values for the afternoons were notably lower for all sites during IOP2 when irrigation was widespread. However, nonirrigated ISS2 and irrigated ISS3 observed the highest and one of the lowest LCL deficit values, respectively. Compared to IOP1 and overall, HI_{low} values were favorably lower during IOP2. The irrigated ISS3 and DOW8 sites observed two of the lowest values of HI_{low} in the morning and afternoon, indicating more favorable conditions for convection over irrigated land use.

The role of cloud cover and time of day was also considered in the context of L–A interactions. Differences in CTP between irrigated and nonirrigated sites were statistically significant for both clear mornings and clear afternoons, where CTP values were higher for irrigated land use than for nonirrigated land use. For clear afternoons, HI_{low} was favorably lower over irrigated land use than nonirrigated land use. For nonclear mornings and afternoons, observed differences for CTP and HI_{low} over irrigated and nonirrigated land uses were statistically not significant. However, the LCL deficits during nonclear mornings were statistically significantly different, with irrigated land use observing a lower LCL deficit than nonirrigated land use. Again, it is evident that under clear conditions irrigated land use provides a more favorable environment for convective development. After further analyzing the coupling metrics by IOPs, cloud cover, and time of day, results show similar impacts. Based on the CTP and LCL deficit, it can be noted that even under nonclear conditions (i.e., under large-scale synoptic influence) the influence of irrigation for convective development is noticeable.

Overall, there is one sustained factor that influenced these three L–A coupling metrics and thus the convective environment: irrigation and the related increase in surface moisture. Increases in surface moisture lead to increases in CTP and favorable decreases in HI_{low} and LCL deficit over irrigated land

use. The impacts of irrigation are most prominent during IOP2 (in other words the peak growing period) when the application of irrigation increases, leading to increased soil moisture. It is clear that land use and vegetation cover/crop growth phases (represented by IOP1 and IOP2) are a dominant influence on L–A interactions and altered convective potential.

5. Summary remarks

LULCC and substantial irrigation expansion took place during the second half of the twentieth century in Nebraska and elsewhere. To better understand the impacts of irrigation on L–A interactions, the GRAINEX field campaign was conducted. The data from the field campaign were used to calculate three L–A coupling/interaction metrics, including CTP, HI_{low}, and LCL deficit to quantify the influence of irrigated and nonirrigated land uses on the lower atmosphere and convection.

Composites of CTP, HI_{low}, and LCL deficits were calculated for two 15-day periods of the growing season of 2018. Over 1000 soundings launched over these two periods (total of 30 days) were used to calculate CTP, HI_{low}, and LCL deficit. As shown in Table 2, these calculations (i.e., metrics) were then grouped by IOP (IOP1 and IOP2), cloud cover (clear and nonclear days), cloud cover (clear and nonclear days during IOP1 and IOP2), time of day, time of day (morning and afternoon) for IOP1 and IOP2, and time of day (morning and afternoon) for clear and nonclear days, and time of day (morning and afternoon) for clear and nonclear days during IOP1 and IOP2. The analyses were completed to further understand the land surface influence on the convective environment. We recognize that in some cases, "clean" separation of clear versus nonclear days may not be as clean. Nonetheless, we are confident that our results are satisfactory because they agree with the conceptual understanding of L–A interactions under irrigated and nonirrigated land uses.

This study finds that with higher CTP, lower HI_{low}, and lower LCL deficit, irrigated land use will yield a more favorable environment for convection. When separated by IOPs, HI_{low} was found to be lower for irrigated cropland than for nonirrigated land use (Table 3). When separated by cloud cover, CTP values were found to be higher over irrigated cropland than nonirrigated land use. Compared to nonirrigated land use, LCL deficits during the peak growing season (IOP2) are favorably lower over irrigated land use, which is conducive for convection (Tables 4–6). Figure 9 summarizes the findings of this research.

Irrigation's relationship with weather and climate is complex, but the observations from GRAINEX and analyses completed for this research have made this relationship clearer. However, further analysis of GRAINEX data and supporting mesoscale modeling research needs to be undertaken to gather new insight into mesoscale circulations in the context of LULCC and irrigation. In addition, a "climatology" is established for one growing season. Analysis of data for additional growing seasons would be helpful to better understand the connections between irrigation, land use, and convection.

In this vein, nocturnal convection is common for south-central and southeast Nebraska (Reif and Bluestein 2017; Geerts et al. 2017). It is shown in this and other GRAINEX data-based studies (Rappin et al. 2021; Lachenmeier et al. 2024) that irrigation can result in higher near-surface and lower-tropospheric moisture content. We suggest that the elevated moisture content due to irrigation may potentially interact with nocturnal processes and impact nocturnal convection. The radiosonde observations during GRAINEX were primarily focused on daytime. In the future, new research using nighttime observations would assist in further understanding the role of irrigation on nocturnal convection. Future research may also include modeling studies to understand the impacts of irrigation on selected and representative weather conditions. Moreover, seasonal-scale modeling research needs to be undertaken to better understand the downstream impacts of irrigation on precipitation.

Acknowledgments. The authors thank three anonymous reviewers for their valuable feedback which helped to improve this manuscript. This research is funded by the National Science Foundation (NSF) Grants AGS-1853390 (Rezaul Mahmood and Eric Rappin), AGS-1720477 (Udaysankar Nair), and AGS-1552487 (Roger Pielke Sr.). Mention of trade names or commercial products in this publication is solely for the purpose of providing specific information and does not imply recommendation or endorsement by the U.S. Department of Agriculture. USDA is an equal opportunity provider and employer.

Data availability statement. Data used in this study can be found at https://www.eol.ucar.edu/field_projects/grainex.

REFERENCES

Adegoke, J. O., R. A. Pielke Sr., J. Eastman, R. Mahmood, and K. G. Hubbard, 2003: Impact of irrigation of midsummer surface fluxes and temperature under dry synoptic conditions: A regional atmospheric model study of the U.S. High Plains. *Mon. Wea. Rev.*, **131**, 556–564, https://doi.org/10.1175/1520-0493(2003)131<0556:IOIOMS>2.0.CO;2.

Alter, R. E., E.-S. Im, and E. A. B. Eltahir, 2015: Rainfall consistently enhanced around the Gezira scheme in East Africa due to irrigation. *Nat. Geosci.*, **8**, 763–767, https://doi.org/10.1038/ngeo2514.

——, H. C. Douglas, J. M. Winter, and E. A. Eltahir, 2018: Twentieth century regional climate change during the summer in the central United States attributed to agricultural intensification. *Geophys. Res. Lett.*, **45**, 1586–1594, https://doi.org/10.1002/2017GL075604.

Barnston, A. G., and P. T. Schickedanz, 1984: The effect of irrigation on warm season precipitation in the Southern Great Plains. *J. Climate Appl. Meteor.*, **23**, 865–888, https://doi.org/10.1175/1520-0450(1984)023<0865:TEOIOW>2.0.CO;2.

Berg, A., K. Findell, B. R. Lintner, P. Gentine, and C. Kerr, 2013: Precipitation sensitivity to surface heat fluxes over North America in reanalysis and model data. *J. Hydrometeor.*, **14**, 722–743, https://doi.org/10.1175/JHM-D-12-0111.1.

Betts, A. K., and J. H. Ball, 1998: FIFE surface climate and site-average dataset 1987–89. *J. Atmos. Sci.*, **55**, 1091–1108,

https://doi.org/10.1175/1520-0469(1998)055<1091:FSCASA>2.0.CO;2.

Bonfils, C., and D. Lobell, 2007: Empirical evidence for a recent slowdown in irrigation-induced cooling. *Proc. Natl. Acad. Sci. USA*, **104**, 13 582–13 587, https://doi.org/10.1073/pnas.0700144104.

Chen, L., and P. A. Dirmeyer, 2019: Global observed and modelled impacts of irrigation on surface temperature. *Int. J. Climatol.*, **39**, 2587–2600, https://doi.org/10.1002/joc.5973.

Christy, J. R., W. B. Norris, K. Redmond, and K. P. Gallo, 2006: Methodology and results of calculating central California surface temperature trends: Evidence of human-induced climate change? *J. Climate*, **19**, 548–563, https://doi.org/10.1175/JCLI3627.1.

Cook, B. I., M. J. Puma, and N. Y. Krakauer, 2011: Irrigation induced surface cooling in the context of modern and increased greenhouse gas forcing. *Climate Dyn.*, **37**, 1587–1600, https://doi.org/10.1007/s00382-010-0932-x.

——, S. P. Shukla, M. J. Puma, and L. S. Nazarenko, 2015: Irrigation as an historical climate forcing. *Climate Dyn.*, **44**, 1715–1730, https://doi.org/10.1007/s00382-014-2204-7.

——, S. S. McDermid, M. J. Puma, A. P. Williams, R. Seager, M. Kelley, L. Nazarenko, and I. Aleinov, 2020: Divergent regional climate consequences of maintaining current irrigation rates in the 21st century. *J. Geophys. Res. Atmos.*, **125**, e2019JD031814, https://doi.org/10.1029/2019JD031814.

DeAngelis, A., F. Dominguez, Y. Fan, A. Robock, M. D. Kustu, and D. Robinson, 2010: Evidence of enhanced precipitation due to irrigation over the Great Plains of the United States. *J. Geophys. Res.*, **115**, D15115, https://doi.org/10.1029/2010JD013892.

Eltahir, E. A. B., 1998: A soil moisture–rainfall feedback mechanism: 1. Theory and observations. *Water Resour. Res.*, **34**, 765–776, https://doi.org/10.1029/97WR03499.

EOL, 2020: GRAINEX: The Great Plains Irrigation Experiment. UCAR/NCAR, accessed 11 June 2022, https://www.eol.ucar.edu/field_projects/grainex.

Fan, X., Z. Ma, Q. Yang, Y. Han, R. Mahmood, and Z. Zheng, 2015a: Land use/land cover changes and regional climate over the Loess Plateau during 2001–2009. Part I: Observed evidences. *Climatic Change*, **129**, 427–440, https://doi.org/10.1007/s10584-014-1069-4.

——, ——, ——, ——, and ——, 2015b: Land use/land cover changes and regional climate over the Loess Plateau during 2001–2009. Part II: Interrelationship from observations. *Climatic Change*, **129**, 441–455, https://doi.org/10.1007/s10584-014-1068-5.

Ferguson, C. R., and E. F. Wood, 2011: Observed land–atmospheric coupling from satellite remote sensing and reanalysis. *J. Hydrometeor.*, **12**, 1221–1254, https://doi.org/10.1175/2011JHM1380.1.

Findell, K. L., and E. A. B. Eltahir, 2003a: Atmospheric controls on soil moisture-boundary layer interactions. Part I: Framework development. *J. Hydrometeor.*, **4**, 552–569, https://doi.org/10.1175/1525-7541(2003)004<0552:ACOSML>2.0.CO;2.

——, and ——, 2003b: Atmospheric controls on soil moisture-boundary layer interactions. Part II: Feedbacks within the continental United States. *J. Hydrometeor.*, **4**, 570–583, https://doi.org/10.1175/1525-7541(2003)004<0570:ACOSML>2.0.CO;2.

——, and ——, 2003c: Atmospheric controls on soil moisture-boundary layer interactions: Three-dimensional wind effects. *J. Geophys. Res.*, **108**, 8385, https://doi.org/10.1029/2001JD001515.

Flanagan, P. X., R. Mahmood, T. Sohl, M. Svoboda, B. Wardlow, M. Hayes, and E. Rappin, 2021: Simulated atmospheric response to four projected land-use land-cover change scenarios for 2050 in the north-central United States. *Earth Interact.*, **25**, https://doi.org/10.1175/EI-D-20-0019.1.

Ford, T. W., A. D. Rapp, and S. M. Quiring, 2015a: Does afternoon precipitation occur preferentially over dry or wet soils in Oklahoma? *J. Hydrometeor.*, **16**, 874–888, https://doi.org/10.1175/JHM-D-14-0005.1.

——, ——, ——, and J. Blake, 2015b: Soil moisture–precipitation coupling: Observations from the Oklahoma Mesonet and underlying physical mechanisms. *Hydrol. Earth Syst. Sci.*, **19**, 3617–3631, https://doi.org/10.5194/hess-19-3617-2015.

Frye, J. D., and T. L. Mote, 2010: Convection initiation along soil moisture boundaries in the Southern Great Plains. *Mon. Wea. Rev.*, **138**, 1140–1151, https://doi.org/10.1175/2009MWR2865.1.

Geerts, B., and Coauthors, 2017: The 2015 Plains Elevated Convection At Night field project. *Bull. Amer. Meteor. Soc.*, **98**, 767–786, https://doi.org/10.1175/BAMS-D-15-00257.1.

Harding, K. J., and P. K. Snyder, 2012a: Modeling the atmospheric response to irrigation in the Great Plains. Part I: General impacts on precipitation and the energy budget. *J. Hydrometeor.*, **13**, 1667–1686, https://doi.org/10.1175/JHM-D-11-098.1.

——, and ——, 2012b: Modeling the atmospheric response to irrigation in the Great Plains. Part II: The precipitation of irrigated water and changes in precipitation recycling. *J. Hydrometeor.*, **13**, 1687–1703, https://doi.org/10.1175/JHM-D-11-099.1.

Holt, T. R., D. Niyogi, F. Chen, K. Manning, M. A. LeMone, and A. Qureshi, 2006: Effect of land–atmosphere interactions on the IHOP 24–25 May 2002 convection case. *Mon. Wea. Rev.*, **134**, 113–133, https://doi.org/10.1175/MWR3057.1.

Hu, Z., Z. Xu, Z. Ma, R. Mahmood, and Z. Yang, 2019: Potential surface hydrologic responses to increases in greenhouse gas concentrations and land use and land cover changes. *Int. J. Climatol.*, **39**, 814–827, https://doi.org/10.1002/joc.5844.

Kang, S., and E. A. B. Eltahir, 2019: Impact of irrigation on regional climate over Eastern China. *Geophys. Res. Lett.*, **46**, 5499–5505, https://doi.org/10.1029/2019GL082396.

Lachenmeier, E., and Coauthors, 2024: Irrigated agriculture significantly modifies seasonal boundary layer atmosphere and lower tropospheric convective environment. *J. Appl. Meteor. Climatol.*, **63**, 245–262, https://doi.org/10.1175/JAMC-D-23-0020.1.

Lawston, P. M., J. A. Santanello Jr., B. F. Zaitchik, and M. Rodell, 2015: Impact of irrigation methods on land surface model spinup and initialization of WRF Forecasts. *J. Hydrometeor.*, **16**, 1135–1154, https://doi.org/10.1175/JHM-D-14-0203.1.

——, ——, B. Hanson, and K. Arsensault, 2020: Impacts of irrigation on summertime temperatures in the Pacific Northwest. *Earth Interact.*, **24**, https://doi.org/10.1175/EI-D-19-0015.1.

Lawston-Parker, P., J. A. Santanello Jr., and N. W. Chaney, 2023: Investigating the response of land–atmosphere interactions and feedbacks to spatial representation of irrigation in a coupled modeling framework. *Hydrol. Earth Syst. Sci.*, **27**, 2787–2805, https://doi.org/10.5194/hess-27-2787-2023.

Leeper, R., R. Mahmood, and A. I. Quintanar, 2011: Influence of karst landscape on planetary boundary layer atmosphere: A

Weather Research and Forecasting (WRF) Model–based investigation. *J. Hydrometeor.*, **12**, 1512–1529, https://doi.org/10.1175/2011JHM1260.1.

Lobell, D. B., and C. Bonfils, 2008: The effect of irrigation on regional temperatures: A spatial and temporal analysis of trends in California. *J. Climate*, **21**, 2063–2071, https://doi.org/10.1175/2007JCLI1755.1.

Mahmood, R., and K. G. Hubbard, 2002: Anthropogenic land-use change in the North American tall grass-short grass transition and modification of near-surface hydrologic cycle. *Climate Res.*, **21**, 83–90, https://doi.org/10.3354/cr021083.

——, ——, and C. Carlson, 2004: Modification of growing season surface temperature records in the northern Great Plains due to land use transformation: Verification of modeling results and implication for global climate change. *Int. J. Climatol.*, **24**, 311–327, https://doi.org/10.1002/joc.992.

——, S. A. Foster, T. Keeling, K. G. Hubbard, C. Carlson, and R. Leeper, 2006: Impacts of irrigation on 20th century temperature in the northern Great Plains. *Global Planet. Change*, **54** (1–2), 1–18, https://doi.org/10.1016/j.gloplacha.2005.10.004.

——, K. G. Hubbard, R. D. Leeper, and S. A. Foster, 2008: Increase in near-surface atmospheric moisture content due to land use changes: Evidence from the observed dew point temperature data. *Mon. Wea. Rev.*, **136**, 1554–1561, https://doi.org/10.1175/2007MWR2040.1.

——, and Coauthors, 2010: Impacts of land use/land cover change on climate and future research priorities. *Bull. Amer. Meteor. Soc.*, **91**, 37–46, https://doi.org/10.1175/2009BAMS2769.1.

——, R. Leeper, and A. I. Quintanar, 2011: Sensitivity of planetary boundary layer atmosphere to historical and future changes of land use/land cover, vegetation fraction, and soil moisture in western Kentucky, USA. *Global Planet. Change*, **78**, 36–53, https://doi.org/10.1016/j.gloplacha.2011.05.007.

——, A. Littell, K. G. Hubbard, and J. You, 2012: Observed data-based assessment of relationships among soil moisture at various depths, precipitation, and temperature. *Appl. Geogr.*, **34**, 255–264, https://doi.org/10.1016/j.apgeog.2011.11.009.

——, T. Keeling, S. A. Foster, and K. G. Hubbard, 2013: Did irrigation impact 20th century air temperature in the High Plains aquifer region? *Appl. Geogr.* **38**, 11–21, https://doi.org/10.1016/j.apgeog.2012.11.002.

——, and Coauthors, 2014: Land cover changes and their biogeophysical effects on climate. *Int. J. Climatol.*, **34**, 929–953, https://doi.org/10.1002/joc.3736.

McDermid, S., and Coauthors, 2023: Irrigation in the Earth system. *Nat. Rev. Earth Environ.*, **4**, 435–453, https://doi.org/10.1038/s43017-023-00438-5.

——, C. Montes, B. I. Cook, M. J. Puma, N. Y. Kiang, and I. Aleinov, 2019: The sensitivity of land–atmosphere coupling to modern agriculture in the northern midlatitudes. *J. Climate*, **32**, 465–484, https://doi.org/10.1175/JCLI-D-17-0799.1.

——, R. Mahmood, M. J. Hayes, J. E. Bell, and Z. Lieberman, 2021: Minimizing trade-offs for sustainable irrigation. *Nat. Geosci.*, **14**, 706–709, https://doi.org/10.1038/s41561-021-00830-0.

McPherson, R. A., 2007: A review of vegetation—atmosphere interactions and their influences on mesoscale phenomena. *Prog. Phys. Geogr.*, **31**, 261–285, https://doi.org/10.1177/0309133307079055.

Mueller, N. D., E. E. Butler, K. A. McKinnon, A. Rhines, M. Tingley, N. M. Holbrook, and P. Huybers, 2016: Cooling of US Midwest summer temperature extremes from cropland intensification. *Nat. Climate Change*, **6**, 317–322, https://doi.org/10.1038/nclimate2825.

——, A. Rhines, E. E. Butler, D. K. Ray, S. Siebert, N. M. Holbrook, and P. Huybers, 2017: Global relationships between cropland intensification and summer temperature extremes over the last 50 years. *J. Climate*, **30**, 7505–7528, https://doi.org/10.1175/JCLI-D-17-0096.1.

Nair, U. S., and Coauthors, 2019: Influence of land cover and soil moisture based brown ocean effect on an extreme rainfall event from a Louisiana gulf coast tropical system. *Sci. Rep.*, **9**, 17136, https://doi.org/10.1038/s41598-019-53031-6.

NASA, 2021: Worldview. Accessed 15 November 2021, https://worldview.earthdata.nasa.gov/.

National Centers for Environmental Information, 2022: Radar. NOAA/NCEI, accessed 29 September 2022, https://www.ncei.noaa.gov/products/radar.

NCAR Earth Observing Laboratory, 1990: NCAR Integrated Surface Flux System (ISFS). NSF NCAR–Earth Observing Laboratory, accessed 17 February 2017, https://doi.org/10.5065/D6ZC80XJ.

——, 1977: Integrated Sounding System (ISS). NSF NCAR–Earth Observing Laboratory, accessed 17 February 2017, https://doi.org/10.5065/D6348HF9.

Ookouchi, Y., M. Segal, R. C. Kessler, and R. A. Pielke, 1984: Evaluation of soil moisture effects on the generation and modification of mesoscale circulations. *Mon. Wea. Rev.*, **112**, 2281–2292, https://doi.org/10.1175/1520-0493(1984)112<2281:EOSMEO>2.0.CO;2.

Pei, L., N. Moore, S. Zhong, A. D. Kendall, Z. Gao, and D. W. Hyndman, 2016: Effects of irrigation on summer precipitation over the United States. *J. Climate*, **29**, 3541–3558, https://doi.org/10.1175/JCLI-D-15-0337.1.

Phillips, C. E., U. S. Nair, R. Mahmood, E. Rappin, and R. A. Pielke Sr., 2022: Influence of irrigation on diurnal mesoscale circulations: Results from GRAINEX. *Geophys. Res. Lett.*, **49**, e2021GL096822, https://doi.org/10.1029/2021GL096822.

Pielke, R. A., and X. Zeng, 1989: Influence on severe storm development of irrigated land. *Natl. Wea. Dig.*, **14**, 16–17.

Pielke, R. A., Sr., and Coauthors, 2011: Land use/land cover changes and climate: Modeling analysis and observational evidence. *Wiley Interdiscip. Rev.: Climate Change*, **2**, 828–850, https://doi.org/10.1002/wcc.144.

——, R. Mahmood, and C. McAlpine, 2016: Land's complex role in climate change. *Phys. Today*, **69**, 40–46, https://doi.org/10.1063/PT.3.3364.

Puma, M. J., and B. I. Cook, 2010: Effects of irrigation on global climate during the 20th century. *J. Geophys. Res.*, **115**, D16120, https://doi.org/10.1029/2010JD014122.

Rappin, E., and Coauthors, 2021: The Great Plains Irrigation Experiment (GRAINEX). *Bull. Amer. Meteor. Soc.*, **102**, E1756–E1785, https://doi.org/10.1175/BAMS-D-20-0041.1.

Rappin, E. D., R. Mahmood, U. S. Nair, and R. A. Pielke Sr., 2022: Land-atmosphere interactions during GRAINEX: Planetary boundary layer evolution in the presence of irrigation. *J. Hydrometeor.*, **23**, 1401–1417, https://doi.org/10.1175/JHM-D-21-0160.1.

Reif, D. W., and H. B. Bluestein, 2017: A 20-year climatology of nocturnal convection initiation over the central and southern Great Plains during the warm season. *Mon. Wea. Rev.*, **145**, 1615–1639, https://doi.org/10.1175/MWR-D-16-0340.1.

Rodgers, W., R. Mahmood, R. Leeper, and J. Yan, 2018: Land cover change, surface mining, and their impacts on a heavy

rain event in the Appalachia. *Ann. Amer. Assoc. Geogr.*, **108**, 1187–1209, https://doi.org/10.1080/24694452.2018.1460249.

Roundy, J. K., and J. A. Santanello, 2017: Utility of satellite remote sensing for land–atmosphere coupling and drought metrics. *J Hydrometeor.*, **18**, 863–877, https://doi.org/10.1175/JHM-D-16-0171.1.

Santanello, J. A., Jr., M. A. Friedl, and M. B. Ek, 2007: Convective planetary boundary layer interactions with the land surface at diurnal time scales: Diagnostics and feedbacks. *J. Hydrometeor.*, **8**, 1082–1097, https://doi.org/10.1175/JHM614.1.

——, C. D. Peters-Lidard, S. V. Kumar, C. Alonge, and W.-K. Tao, 2009: A modeling and observational framework for diagnosing local land–atmosphere coupling on diurnal time scales. *J. Hydrometeor.*, **10**, 577–599, https://doi.org/10.1175/2009JHM1066.1.

——, ——, and ——, 2011: Diagnosing the sensitivity of local land-atmosphere coupling via the soil moisture-boundary layer interaction. *J. Hydrometeor.*, **12**, 766–786, https://doi.org/10.1175/JHM-D-10-05014.1.

——, ——, A. Kennedy, and S. V. Kumar, 2013: Diagnosing the nature of land-atmosphere coupling: A case study of dry/wet extremes in the U.S. Southern Great Plains. *J. Hydrometeor.*, **14**, 3–24, https://doi.org/10.1175/JHM-D-12-023.1.

——, and Coauthors, 2018: Land–atmosphere interactions: The LoCo perspective. *Bull. Amer. Meteor. Soc.*, **99**, 1253–1272, https://doi.org/10.1175/BAMS-D-17-0001.1.

——, P. Lawston, S. V. Kumar, and E. Dennis, 2019: Understanding the impacts of soil moisture initial conditions on NWP in the context of land–atmosphere coupling. *J. Hydrometeor.*, **20**, 793–819, https://doi.org/10.1175/JHM-D-18-0186.1.

Schlemmer, L., C. Hohenegger, J. Schmidli, C. S. Bretherton, and C. Schär, 2011: An Idealized cloud-resolving framework for the study of midlatitude diurnal convection over land. *J. Atmos. Sci.*, **68**, 1041–1057, https://doi.org/10.1175/2010JAS3640.1.

——, ——, ——, and C. Schär, 2012: Diurnal equilibrium convection and land surface–atmosphere interactions in an idealized cloud-resolving model. *Quart. J. Roy. Meteor. Soc.*, **138**, 1526–1539, https://doi.org/10.1002/qj.1892.

Segal, M., R. Avissar, M. C. McCumber, and R. A. Pielke, 1988: Evaluation of vegetation effects on the generation and modification of mesoscale circulations. *J. Atmos. Sci.*, **45**, 2268–2293, https://doi.org/10.1175/1520-0469(1988)045<2268:EOVEOT>2.0.CO;2.

Sen Roy, S., R. Mahmood, D. Niyogi, M. Lei, S. A. Foster, K. G. Hubbard, E. Douglas, and R. A. Pielke Sr., 2007: Impacts of the agricultural green revolution–induced land use changes on air temperatures in India. *J. Geophys. Res.*, **112**, D21108, https://doi.org/10.1029/2007JD008834.

——, ——, A. I. Quintanar, and A. Gonzalez, 2011: Impacts of irrigation on dry season precipitation in India. *Theor. Appl. Climatol.*, **104**, 193–207, https://doi.org/10.1007/s00704-010-0338-z.

Shukla, S. P., M. J. Puma, and B. I. Cook, 2014: The response of the South Asian summer monsoon circulation to intensified irrigation in global climate model simulations. *Climate Dyn.*, **42**, 21–36, https://doi.org/10.1007/s00382-013-1786-9.

Singh, D., S. P. McDermid, B. I. Cook, M. J. Puma, L. Nazarenko, and M. Kelley, 2018: Distinct influences of land cover and land management on seasonal climate. *J. Geophys. Res. Atmos.*, **123**, 12 017–12 039, https://doi.org/10.1029/2018JD028874.

Suarez, A., R. Mahmood, A. I. Quintanar, A. Beltran-Przekurat, and R. A. Pielke Sr., 2014: A comparison of the MM5 and the regional atmospheric modeling system simulations for land–atmosphere interactions under varying soil moisture. *Tellus*, **66A**, 21486, https://doi.org/10.3402/tellusa.v66.21486.

Szilagyi, J., and T. E. Franz, 2020: Anthropogenic hydrometeorological changes at a regional scale: Observed irrigation–precipitation feedback (1979–2015) in Nebraska, USA. *Sustainable Water Resour. Manage.*, **6**, 1, https://doi.org/10.1007/s40899-020-00368-w.

Taylor, C. M., 2010: Feedbacks on convection from an African wetland. *Geophys. Res. Lett.*, **37**, L05406, https://doi.org/10.1029/2009GL041652.

Wei, J., P. A. Dirmeyer, D. Wisser, M. C. Bosilovich, and D. M. Mocko, 2013: Where does the irrigation water go? An estimate of the contribution of irrigation to precipitation using MERRA. *J. Hydrometeor.*, **14**, 275–289, https://doi.org/10.1175/JHM-D-12-079.1.

Winchester, J., R. Mahmood, W. Rodgers, F. Hossain, E. Rappin, J. Durkee, and T. Chronis, 2017: A model-based assessment of potential impacts of man-made reservoirs on precipitation. *Earth Interact.*, **21**, https://doi.org/10.1175/EI-D-16-0016.1.

Wurman, J., and Coauthors, 2021: The Flexible Array of Radars and Mesonets (FARM). *Bull. Amer. Meteor. Soc.*, **102**, E1499–E1525, https://doi.org/10.1175/BAMS-D-20-0285.1.

Xu, Z., R. Mahmood, Z.-L. Yang, C. Fu, and H. Su, 2015: Investigating diurnal and seasonal climatic response to land use and land cover change over monsoon Asia with the Community Earth System Model. *J. Geophys. Res. Atmos.*, **120**, 1137–1152, https://doi.org/10.1002/2014JD022479.

Yang, Z., and Coauthors, 2019: Irrigation impact on water and energy cycle during dry years over the United States using convection-permitting WRF and a dynamical recycling model. *J. Geophys. Res. Atmos.*, **124**, 11 220–11 241, https://doi.org/10.1029/2019JD030524.

Zhang, T., R. Mahmood, X. Lin, and R. A. Pielke Sr., 2019: Irrigation impacts on minimum and maximum surface moist enthalpy in the Central Great Plains of the USA. *Wea. Climate Extremes*, **23**, 100197, https://doi.org/10.1016/j.wace.2019.100197.